

Spatiotemporal relationships between earthquakes of the Mid-Atlantic Ridge and the Atlantic continental margins

Author: Oluwaseyi Joseph Bolarinwa

Persistent link: <http://hdl.handle.net/2345/bc-ir:104565>

This work is posted on [eScholarship@BC](#),
Boston College University Libraries.

Boston College Electronic Thesis or Dissertation, 2015

Copyright is held by the author, with all rights reserved, unless otherwise noted.

Boston College

The Graduate School of Arts and Sciences

Department of Earth and Environmental Sciences

SPATIOTEMPORAL RELATIONSHIPS BETWEEN EARTHQUAKES
OF THE MID-ATLANTIC RIDGE AND THE ATLANTIC
CONTINENTAL MARGINS.

a thesis

by

OLUWASEYI J. BOLARINWA

Submitted in partial fulfillment of the requirements

For the degree of

Master of Science

August 2015

ABSTRACT

SPATIOTEMPORAL RELATIONSHIPS BETWEEN EARTHQUAKES OF THE MID-ATLANTIC RIDGE AND THE ATLANTIC CONTINENTAL MARGINS.

By Bolarinwa Oluwaseyi J.

Advisors: Professors Ebel and Kafka

The seismicity of the mid Atlantic Ridge (MAR) was compared in space and time with the seismicity along the Atlantic continental margins of Europe, Africa, North America, the Caribbean and South America in a bid to appraise the level of influence of the ridge push force at the MAR on the Atlantic coastal seismicity. By analyzing the spatial and temporal patterns of many earthquakes (along with the patterns in their stress directions) in diverse places with similar tectonic settings, it is hoped that patterns that might be found indicate some of the average properties of the forces that are causing the earthquakes. The spatial analysis of the dataset set used shows that areas with higher seismic moment release along the north MAR spatially correlate with areas with relatively lower seismic moment release along the north Atlantic continental margins (ACM) and vice versa. This inverse spatial correlation observed between MAR seismicity and ACM seismicity might be due to the time (likely a long time) it takes stress changes from segments of the MAR currently experiencing high seismic activity to propagate to the associated passive margin areas presently experiencing relatively low seismic activity. Furthermore, the number of Atlantic basin and Atlantic coast earthquakes occurring away from the MAR is observed to be independent of the proximity of earthquake's epicenters from the MAR axis. The effect of local stress as noted by Wyssession et al. (1995) might have contributed to the independence of Atlantic

basin and Atlantic coast earthquake proximity from the MAR. The Latchman (2011) observation of strong earthquakes on a specific section of the MAR being followed by earthquakes on Trinidad and Tobago was tested on other areas of the MAR and ACM. It was found that that the temporal delay observed by Latchman does not exist for the seismicity along other areas along the MAR and ACM. Within the time window used for this study, it appears that seismicity is occurring randomly in space away from the MAR. The weak anticorrelations between ACM and MAR seismicity show that the ridge push force probably has some level of influence on the ACM seismicity. However, as revealed from previous research on the study area, the forces resulting from lateral density contrasts related to topographic features and lateral density variations between oceanic and continental crust also appear to significantly influence the seismicity of the Atlantic coastal margins.

ACKNOWLEDGEMENT

My ultimate gratitude to God for the gift of life and the knowledge he has afforded me to conduct the research that culminated into this dissertation. I am eternally indebted and grateful to Him. My sincere gratitude to Dr John Ebel, my professor and thesis advisor, for his timely insights and guidance while I pieced together this dissertation. He always urged me to go the extra mile and, in retrospect, it all paid off. Many thanks to Dr Alan Kafka, my co-thesis-advisor, for his assistance in the course of my research and his comments and suggestions while he read through this dissertation.

I really appreciate Marilyn Bibeau, Weston Observatory administrator, for her kindness and love while I worked on my research at the Weston observation. Her motherly attitude still warms my heart as I write this acknowledgement. The academic and moral assistance given me by Justin Starr at the Weston Observatory is very much appreciated. My hearty gratitude to Vanessa Napoli and Yahya Abushaheen and again Justin Starr for their genuine friendship and kind help as they offered me rides to the Observatory in the summer months that I worked on my research. I am very thankful to Tyler Cox for his ever readiness to put me through Matlab while I was still a fledgling programmer.

Daddy, thank you for your moral, spiritual and academic mentorship from my childhood. Thanks for continually teaching me math until you drummed into my subconscious the fundamental building block of mathematics. A world of gratitude and appreciation to my siblings: Olufemi, Oluwatosin and Olufunmilayo; thank you for believing in me and supporting me all through to this point in my academic pursuit.

TABLE OF CONTENTS

1. Introduction.....	1
2. Tectonics of the Study Area.....	4
3. Data.....	16
4. Spatial Analysis.....	20
5. Temporal Analysis.....	30
5.1. Temporal Analysis Procedure and Result.....	30
6. Spatiotemporal Analysis.....	37
7. Discussion.....	43
8. Conclusions.....	46
9. References.....	47

APPENDIX A- Supplemental Figures for Section 3

APPENDIX B- Supplemental Tables for Section 5

1. Introduction

The seismicity of intraplate regions is generally low compared with that at plate boundaries (Johnston, 1989), but the source of stress driving intraplate tectonics may be more complex than that driving the tectonics at plate boundaries (Barros et al., 2009). Oceanic lithosphere that terminates at passive margins moves under the action of two plate driving forces. One force is friction applied to the base of the lithosphere due to convective flow in the asthenosphere and trends in the direction of the convective flow (Kirdyashkin and Kirdyashkin, 2013). The other force is caused by the altitude of the ridge, where gravity acting on the locally elevated topography produces excess pressure that ultimately pushes the lithospheric plate away from the ridge. This force may be called gravitational sliding (Kirdyashkin and Kirdyashkin, 2013), and for the purpose of this study it is referred to as the ridge push force.

Previous studies on intraplate stress orientations along the Atlantic continental margins (ACM) suggest that the ridge push force contributes significantly to the regional stress fields of the Atlantic passive margins (Muller et al., 1992; Assumpcao, 1998; Hurd and Zoback, 2012). For instance, using compiled stress data (made up of 75 earthquake focal mechanisms and 10 formal stress inversions) from the central and eastern United States and southern Canada, Hurd and Zoback (2012) showed that the maximum horizontal compressive stress (S_{Hmax}) across much of intraplate North America is oriented NE-SW. They also reported that these data are consistent with many previous stress measurements, such as those reported in Zoback (1992a), who interpreted the observed regional stress field as due largely to the ridge push force. Along the Atlantic coasts of Europe and South America, studies show that the ridge push force due to gravity sliding

from the Mid Atlantic ridge (MAR) acts on these continental boundaries. The ridge push force at these boundaries is locally modified by the lithospheric properties in different regions, regional stresses, local flexural effects from thick sedimentary loads, and a presumably weaker crust from Mesozoic thinning that all contribute to intraplate stress perturbations along these passive margins (Muller et al., 1992; Assumpcao, 1998). Zoback (1992) showed that the ridge push force from the MAR dominates the stress field of western and southern Africa, but for this margin (western/south African margin) no studies have been produced that show stress perturbations due to local effects. The history of the occasional past damaging earthquakes coupled with the steady population growth in the intraplate regions of the ACM (Stewart, 2005) underscores the need to better understand the causes of earthquakes in these regions.

In order to investigate possible causality between MAR seismicity and intraplate seismicity along the Atlantic continental margins (ACM), Skordas et al. (1991) looked for a temporal relationship between the seismicity of the North Atlantic Ridge and Fennoscandia. They concluded based on their findings that the observed seismicity patterns indicate a tectonic connection between the two regions. This study explores a broader geographical region than that examined by Skordas et al. (1991). In this thesis I examine the potential contribution of the spreading MAR force to the seismicity along the ACM by looking for correlations between the Mid-Atlantic ridge (MAR) earthquake activity since 1973 and the earthquake activity for the same time period within the Atlantic basin (that is between MAR and ACM) and along the ACM of North America, Europe, Africa, South America and the Caribbean. The dataset used for this study was explored for spatial correlations of the earthquake energy release along the MAR with

corresponding places within the Atlantic basin and also along the ACM on both sides of the Atlantic Ocean. In addition, using the Elsasser (1969) stress diffusion model, potential temporal associations between MAR earthquakes and earthquakes along the ACM were investigated by looking for time lags between large MAR events and ACM events.

2. Tectonics of the Study Area

The margins of continents can be tectonically active or passive. Examples of active continental margins include the Nubian-Somalian boundary where active spreading is happening, the transform portion of the Pacific-North America boundary such as along the San Andreas Fault in California, and the Nazca-South America boundary where the Nazca plate is subducting under the South American plate (Stein and Wysession, 2003). Passive margins are formed by rifting followed by seafloor spreading; the resulting plate is made up of both continental and oceanic lithosphere (Bradley, 2008). The thinning process of the lithosphere during continental rifting can be described in three stages: the first is the extension phase during which the continent is uplifted and some tilted blocks appear, followed by the exhumation phase which is the main thinning phase, and finally the break-up and oceanic spreading phase (Aslanian et al., 2009). There are differences in the morphologies between active and passive margins, and these differences can be ascribed to the processes that control their formation. The morphology of passive margins is controlled by erosion and deposition; active tectonic and magmatic processes shape the morphologies of active margins (Emery, 1980; Uchupi and Emery, 1991). This thesis focuses on continental passive margins that were formed during continental rifting and opening of the Atlantic Ocean.

There have been four cycles of ocean closing and the re-opening that have affected the passive margins of the modern Atlantic Ocean (Anderson, 1982; Goodwin, 1985). The latest cycle started 180 Ma ago at the Gulf of Mexico when a young mid-ocean ridge formed and began to migrate towards the south and north. Later, the opening of the southern end of the South Atlantic began 130 Ma ago, and this rifting migrated

towards the equator (Silveira and Stutzmann, 2002). Together these rifting events acted to form the modern Atlantic Ocean basin. The morphology of the Atlantic has been stable since 33 Ma ago; the MAR is currently spreading at rates that vary between 1 and 4 cm per year (Silveira and Stutzmann, 2002).

Seismicity along the ACM continental shelves and those within a few hundred kilometers landward from the ACM coastlines can be classified as passive margin seismicity (Johnston, 1989) (Figure 1). Along the northeastern ACM, central-west Europe ($43^{\circ}N$ to $54^{\circ}N$) exhibits diffuse seismicity with the largest known earthquakes rarely greater than magnitude 4 (Tesauro et al., 2006). This seismicity seems to be concentrated on old zones of weakness that are reactivated by the present-day stress field (Ziegler, 1992). A large number of the earthquakes in central-west Europe occur at shallow depths (less than 15 km), and most earthquakes in this region are preferentially located along three geologic belts: the Alpine chain, the European Cenozoic rift system and the area that lies between the Armorican Massif and the Massif central (Tesauro et al., 2006). The major seismic activity in western Iberia is found at or close to the Eurasia/Africa boundary, especially in the Goringe bank region. The most active faults onshore in Iberia are the Vilarica fault and the Lower valley of the Tagus fault (Pinheiro et al., 1996).

Along the northwest ACM, both small and large earthquakes of central and eastern North America are primarily located along the rifted margin or along failed rift arms within a few hundred kilometers of the continental margin (Mazzotti and Townend, 2010). Earthquake depths vary in the region. For example, most earthquakes in the northeastern U.S. and the nearby maritime provinces of Canadian occur at focal depths of

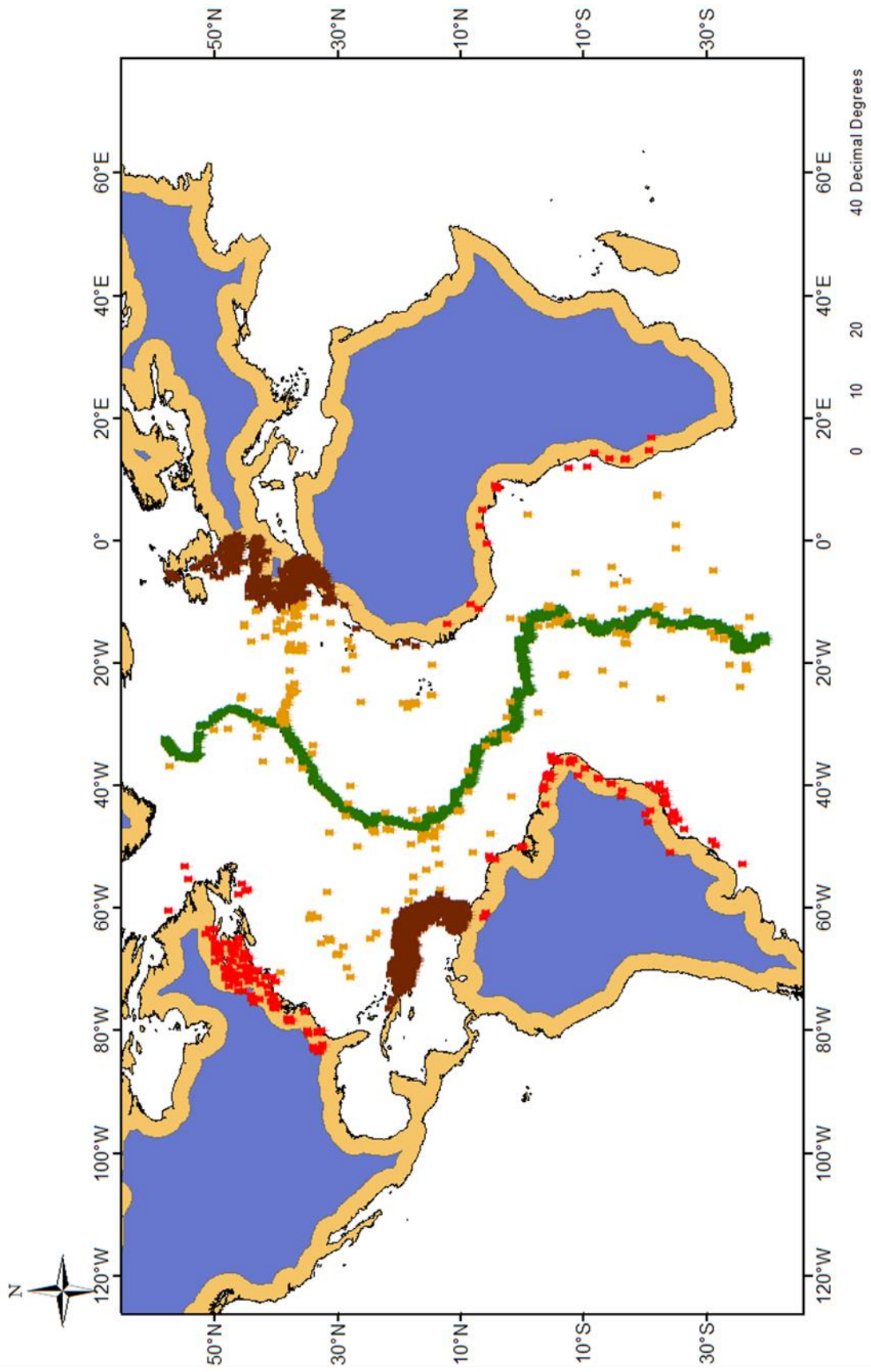


Figure 1: Study Area showing MAR, Atlantic Basin and ACM seismicity. The MAR events are shown in green, the Atlantic Basin events are in yellow. Along the ACM the seismicity of Europe-North Africa and the Caribbean margins are colored in brown while the seismicity of North America, South America and the rest of Africa margins is in red.

10 km or less. Inland within the nearby shield areas of southeastern Canada earthquakes can occur down to a focal depth of about 30 km (Ebel, 1999). In the Appalachian region of the southeastern U.S., earthquakes largely happen below 10 km depth whereas within the accreted terrains along the southeastern U.S. coast the focal depths are usually less than about 10-15 km (Bollinger et al., 1991).

The passive continental margin area of West Africa exhibits low seismicity when compared with the MAR to its west and the East Africa rift system to its east. The most seismically active parts of the ACM of West Africa are the coasts of Guinea and Ghana and the volcanic area of Mt. Cameroon (Ambraseys and Adams, 1986). Large earthquakes (magnitude 5.5 and greater) that have occurred since 1930 in West Africa had focal depths of 15 km and less; these earthquakes displayed large components of strike-slip motion (Suleiman et al., 1992). The faulting in Zaire, Gabon and Cameroon appears to be influenced by the orientation of pre-existing Precambrian basement structures, while the faulting in Ghana and the Gulf of Guinea seems to be controlled by structures related to the breakup of Africa and South America (Suleiman et al., 1992).

Along the southwest ACM earthquakes in the continental region of Brazil preferentially happen in areas of low topography (Assumpcao, 1998). In the northeastern margin of Brazil (north of $10^{\circ}S$), earthquakes happen in the continent with a very low level of seismic activity. Towards the south of $15^{\circ}S$, earthquakes tend to cluster in areas along the continental shelf while there is less seismic activity onshore (Assumpcao, 1998). Earthquakes generally happen at upper crustal depths in the northeastern segment of Brazil (Assumpcao, 1992); the focal depths of earthquakes studied by Assumpcao (1998) along the southeast passive margin of Brazil range from 8 to 18 km.

The state of stress at passive margins is largely comprised of regionally and locally generated stress fields (Zoback, 1992). The regional component of the stress field has been attributed to plate boundary forces that drive plate motion, such as ridge push and slab pull (Richardson, 1992; Zoback, 1992). Second order stress patterns can result from lithospheric flexure and lateral density variation within a plate, such as isostatic compensation, deglaciation and topography (Zoback, 1992; Coblenz et al., 1998; Zoback and Mooney, 2003; Bird et al., 2006).

Continental shelf and coastal earthquakes make up about a third of the seismicity in stable continental crust (Johnston, 1989). Inferences about the state of stress in the earth's crust in a region can be obtained from the fault geometries of earthquakes in the area (Hurd and Zoback, 2012). Using fault plane solutions of earthquakes as a key tool, past studies revealed a compressional crustal stress pattern along the North America passive margin, and the maximum horizontal compressional stress direction tends to orient ENE-WSW (Figures 1 and 2). This stress field has largely been attributed to the ridge push force (Zoback, 1992a; Hurd and Zoback, 2012). On the Western Europe segment of the ACM, Muller et al. (1992) identified three distinct regional patterns of maximum horizontal compressive stress (S_{Hmax}): a consistent NW to NNW S_{Hmax} stress orientation in western Europe; a WNW-ESE S_{Hmax} orientation in Scandinavia; and a consistent E-W S_{Hmax} orientation and N-S extension in the Aegean sea and west Anotalia (Figure 1). They proposed that these different stress fields can be associated with the ridge push force altered locally by variations in the thickness of the elastic lithospheric layers in the different regions.

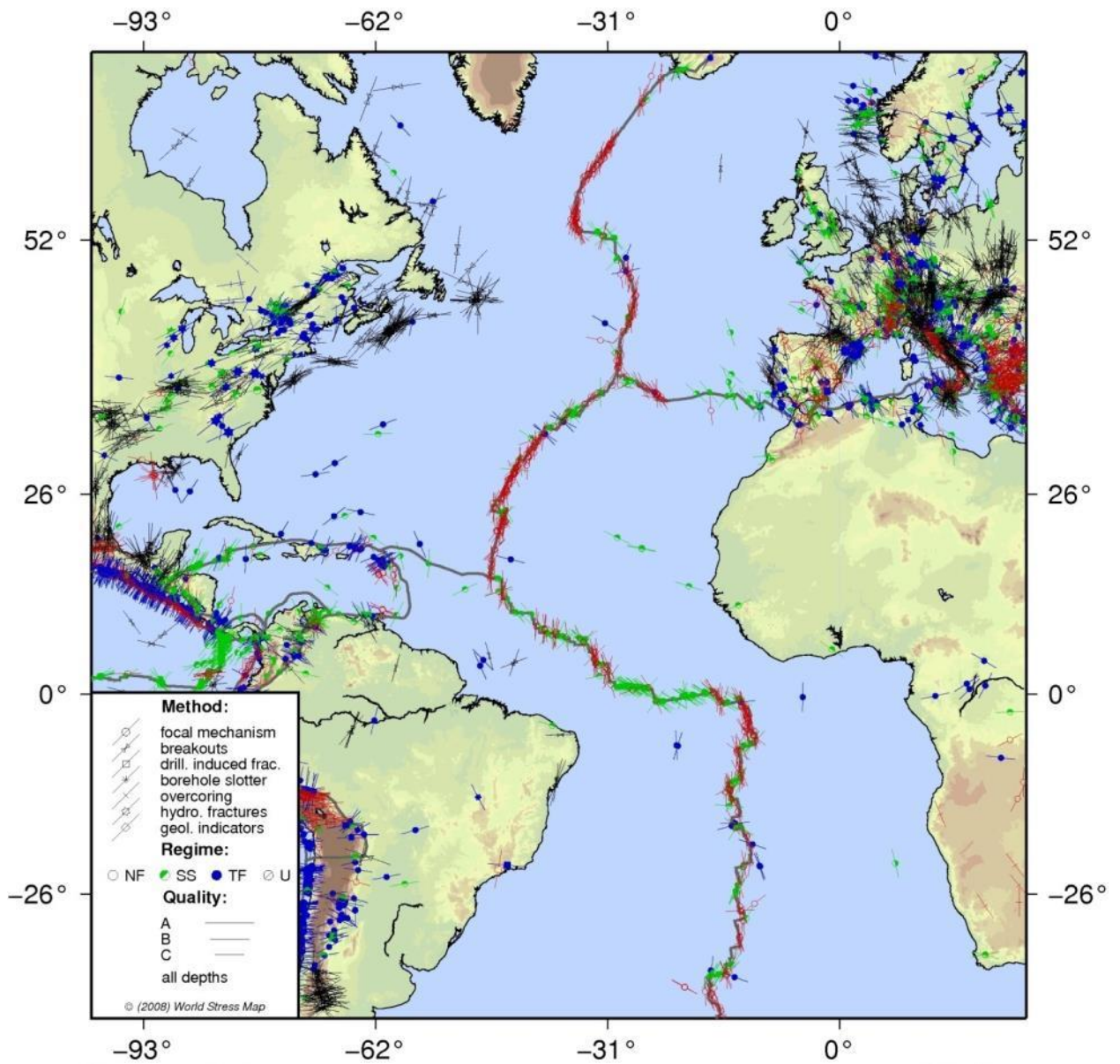


Figure 2: Stress map of the MAR and the Atlantic Coasts (Heidbach et al., 2008).

For the south Atlantic ACM regions Assumpcao (1998) observed different seismicity and stress patterns between the north and south segments of the Brazilian continental margin of South America. To the north, the S_{Hmax} tends to orient parallel to the northeast coastline. On the other hand, along the southeastern segments of the Brazilian continental margin, compressional stress oriented E-W to WNW-ESE is observed offshore (Figure 2). On the east side of the ACM, stress data in central and western Africa suggest that S_{Hmax} orients approximately E-W (Zoback, 1992a; Ayele, 2002). This compressive stress regime could be explained as E-W contraction of the African plate resulting from ridge push forces from the MAR and the East African Rift System (Ayele, 2002).

Brittle failure in most cases happens on preexisting faults (Turcotte et al., 2003). A fault ruptures when the applied shear stress exceeds the fracture strength, which is controlled by the coefficient of static friction (Turcotte et al., 2003). The stress on a fault in the course of the rupture is controlled by the coefficient of dynamic friction. Provided that the coefficient of dynamic friction is less than the coefficient of static friction, stick-slip behavior results and earthquakes happen (Turcotte et al., 2003). With this framework as a guide, the most general question that will be addressed in this study is how plate tectonics might induce earthquakes along the Atlantic passive margins.

There are a couple of difficulties encountered when trying to relate stress in the earth to specific earthquakes. First, stress magnitudes are difficult to measure in the field and therefore are poorly constrained (Freed, 2005). However, principal stress directions can be inferred from well breakouts and earthquake focal mechanisms (Amato et al., 1995; Mariucci and Muller, 2003). Second, models of the seismic cycle incorporate the

buildup of elastic strain within rocks until they are stressed pass their elastic limit (Conrad, 2013; Lillie, 1999), and it is very difficult or impossible to know precisely when the rock will reach its breaking point.

Earthquakes are caused when the shear stress in rocks reaches some threshold level at which failure occurs (McGarr, 1999; Lillie, 1999). The time and epicenter of each earthquake is likely controlled by local perturbations to the stress field along with some random chance of failure (Attewel and Farmer, 1973; Marsan and Bean, 2000).

Therefore, the occurrence of any individual earthquake does not say much about the dynamics that triggered that earthquake. However, by analyzing the spatial and temporal patterns of many earthquakes (along with the patterns in their stress directions) in diverse places with similar tectonic settings, it is hoped that patterns that might be found indicate some of the average properties of the forces that are causing the earthquakes.

The question of how plate tectonics is causing passive margins earthquakes cannot be directly addressed with the data analyzed in this thesis; however, this study aims to address some specific questions about the dynamics of Atlantic passive margin seismicity. Some segments of the MAR have more seismicity when compared to other segments of the MAR (e.g., Smith et al., 2003). Perhaps the more seismically active segments of the MAR are related to active deformation there, and presumably this deformation is related to a stronger ridge push force acting on those segments of the passive margins. If this assertion is true, then perhaps the ACM areas closer to those more active MAR areas also exhibit more seismicity as well. The proposition that local earthquake rates are proportional to local stress changes at the MAR is investigated in this thesis.

Correlations between S_{Hmax} directions and azimuths of absolute and relative plate velocities were presented for several intraplate regions by Zoback et al. (1989) (Figure 3). The absolute velocity trajectories in Figure 3 show the directions of the resultant plate boundary forces causing the plate motion and in turn the stress directions due to the plate boundary forces. As can be seen in Figure 3 the plate boundary stress trajectory at the equatorial MAR parallels the S_{Hmax} directions at the equatorial Atlantic margins; however, for example, in the north Atlantic, the stress trajectory from a point in North America intercepts the MAR at a latitude that is north by several degrees compared to that of the point in North America (Figure 3).

The mean stress path extrapolated from the MAR to the ACM aligns with the S_{Hmax} of the ACM stress orientation in eastern North America, and this information can be used to match the source of the ridge-push force along the MAR to a point along the ACM. Figure 3 shows an example of this. For the site circled in yellow in Figure 3 the point on the MAR where the ridge-push force would be acting is about 7.1° north of the latitude of the ACM site (Figure 3). Thus, to find out if local earthquake rates are proportional to local stress changes at the MAR and that these stress changes are transmitted to the ACM, the ACM seismicity will be spatially compared to that of MAR seismicity at spatial shifts in latitude from 0 to 7° .

During an earthquake, elastic strain energy and gravitational energy stored in the earth are released as radiated energy, fracture energy (resulting from permanent deformation) and thermal energy (Kanamori and Rivera, 2006). The non-radiating component of the potential energy released cannot be measured (Kanamori and Rivera, 2006), but the kinetic energy is communicated globally through elastic seismic waves

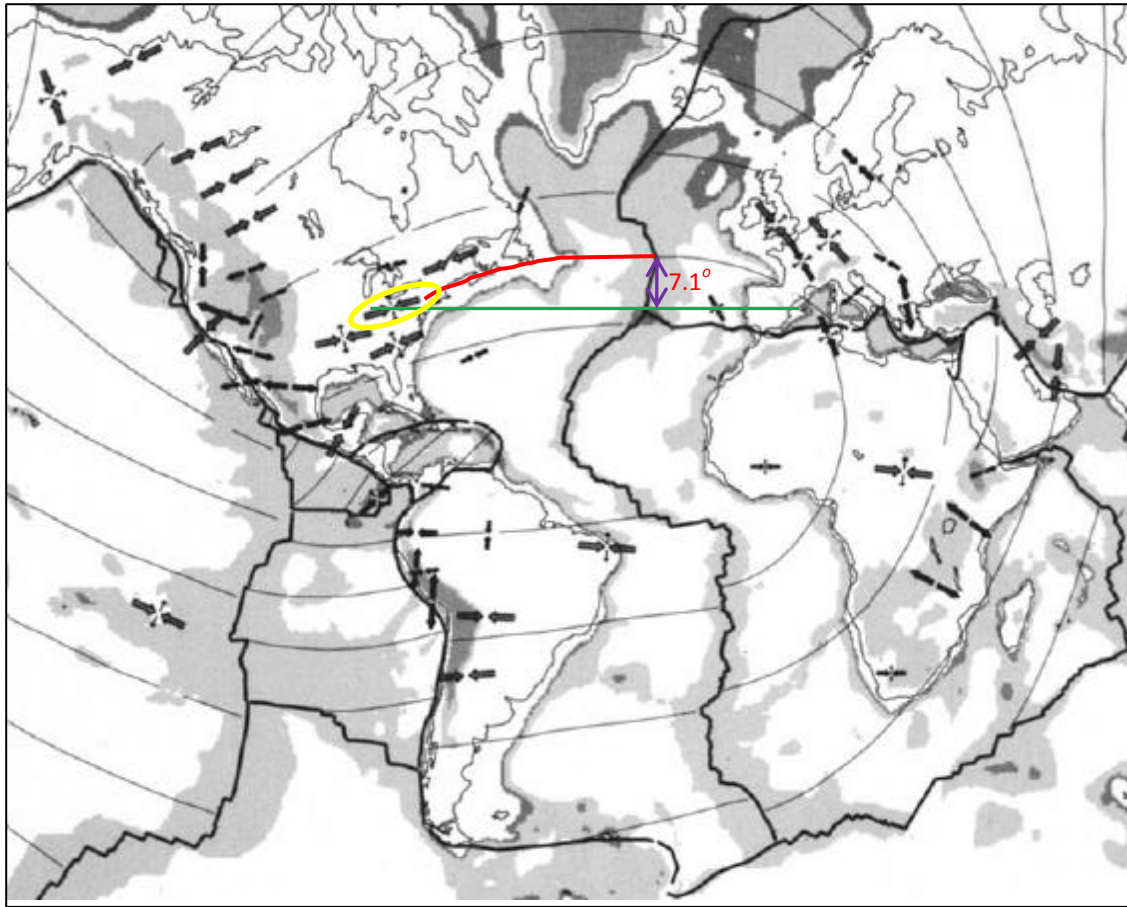


Figure 3: Generalized stressed map showing mean stress directions. The curved lines show the absolute velocity trajectories for each plate based on the AM-2 model of Minster and Jordan (1978). Each single set of thick arrow marks facing each other indicates S_{Hmax} orientation in a thrust faulting stress regime. A single set of thick arrows pointing away from each other represents S_{Hmin} orientation in a normal faulting stress regime. Thick arrow marks pointing towards each other with thin arrow marks pointing away from each other represent strike-slip faulting stress regime (Zoback et al., 1992). A mean stress path is extrapolated from the MAR to the Atlantic margin of North America (drawn in red), and this stress path aligns with the S_{Hmax} of the event circled in yellow along North America Atlantic margin. The angular difference between the intersection of the extrapolated stress path with the MAR axis and an east-west line (colored in green) passing through the arrows of the site circled in yellow is 7.1° .

and the stress diffusion mechanism proposed by Elsasser (1967) and Melosh (1976). Consequently, a second proposition that will be investigated in this thesis is that stress changes at the MAR might travel at elastic wave and stress diffusion rates (minutes to a few years) to the Atlantic passive margins.

Motion at tectonic plate boundaries results from the convective force of the mantle (Tackley, 2000; Bercovici, D. and Ricard, Y. 2000); the dynamics of intraplate earthquakes are more complicated compared to plate boundary earthquakes (Barros et al., 2009). Continental areas like South America, stable North America and Western Europe exhibit maximum horizontal stress orientations that predominantly parallel the directions of absolute plate motions (Zoback et al., 1989; Golke and Coblenz, 1996). From these findings, it was proposed that plate boundary forces (for example, the ridge push force) have a significant control on the strength and direction of intraplate stress fields (Zoback et al., 1989; Zoback and Magee, 1991; Muller et al., 1992; Coblenz and Richardson, 1996). Furthermore, Latchman (2011) observed that earthquakes of magnitudes 6 and greater at the MAR are followed by margin earthquakes (magnitude 5 or larger) near the Island of Tobago within a uniform delay of 39 ± 4 months. In order to find out if stress changes at the MAR might travel at the Latchman (2011) migration rate to the Atlantic passive margins, the temporal aspect of this study will find out if the reported confined match between MAR and ACM seismicity can be seen at other areas of the MAR and ACM. The Elsasser (1969) stress diffusion model will be used to test if oceanic and ACM earthquakes are happening away from the MAR at a rate similar to that reported by Latchman (2011).

If stress diffuses away from the MAR according to the Elsasser model, then there should be evidence of seismicity migration away from the MAR with time. Seismicity migration will be tested by looking at the time history of Atlantic Basin earthquakes following MAR earthquakes. The time-space plot will be used to test if earthquakes closer to the MAR happen earlier relative to those farther away from the MAR when compared in time with prior earthquake events at the MAR.

3. Data

All data used for this study were obtained from the National Earthquake Information Center (NEIC), except the data for the passive margin of South America that was provided by M. Assumpcao (Assumpcao, 1998 and Assumpcao et al., 2011). The Assumpcao catalog was preferred over the NEIC catalog for the South American passive margin because of its completeness magnitude threshold of 3.5, which is lower than that of the NEIC catalog for this region. The two catalogs used for this study cover the MAR from latitude 38°S and 58°N and areas along the extension of the Atlantic fracture zones through the Atlantic basin and the Atlantic margins over a time period of 39 years between 1973 and 2011 (Figure 4). For this study, the ACM is defined as the area within 300 km inland of the coastline and 200 km offshore from the coastline (Figures 1 and 2).

The Atlantic margins are not entirely passive margins; active margins in the study area include the Caribbean-North America plate boundary, the Caribbean-South America plate boundary and the Eurasia-Africa plate boundary (Rosencrantz and Mann, 1991; DeMets et al., 2000; Serpelloni et al., 2007). Along the Eurasia-Africa plate boundary, earthquakes have occurred at depths greater than 500 km (Serpelloni et al., 2007) and along the Caribbean Atlantic margin, earthquakes have occurred at depths greater than 190 km (Russo et al., 1993).

The active subduction margins of the ACM are along the Caribbean Atlantic coast and the Atlantic coast of Iberia (Gutscher et al., 2002; Brink and Lopez-Venegas, 2012). At the active margins, the slab pull force acts in addition to the ridge push force and the drag force that comes from mantle flow beneath the plate (Stefanick and Jurdy, 1992).

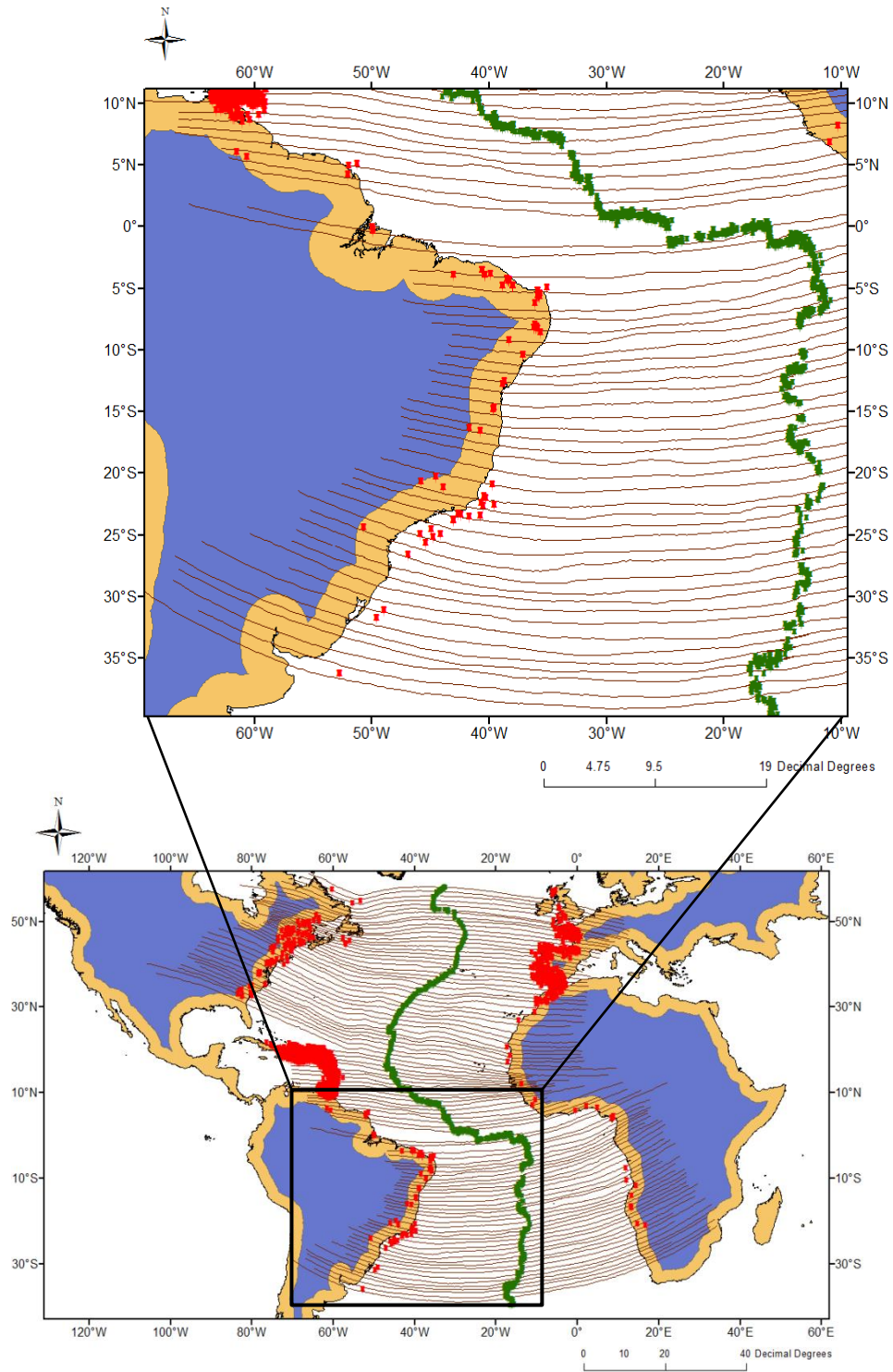


Figure 4: Study area showing the seismicity of the study area and mapped fracture zones of the Atlantic basin onto the Atlantic coasts.

Along passive margins, the ridge push force and mantle flow forces alone act there (Dore et al., 2008). Earthquakes at passive margins typically occur at depths less than 35 km (Gvirtzman, 2002). For this study, only continental crustal events with depth 35 km and less at the Atlantic margins were analyzed because almost all of the ACM area is comprised of passive margins with seismicity at depths of 35 km or less.

To appraise the level of completeness of the earthquake catalogs, I evaluated the magnitude of completeness M_c using the Gutenberg-Richter law. The magnitude of completeness M_c is defined as the lowest magnitude of events that a network is able to record reliably and completely over a time period. At any magnitude below M_c , events likely are missing from the catalog because the network may not detect all events with magnitudes less than M_c (Schorlemmer and Woessner, 2008). Using plots of data fit with the Gutenberg-Richter power law, I estimated the magnitude of completeness as the lowest magnitude on the plot below which the curve diverges from the expected linear relationship between the log of the number of earthquakes $\geq M$ and the body wave magnitude m_b (Gutenberg and Richter, 1944; Appendix A). The Gutenberg-Richter power law is expressed in the equation

$$\log N = a - bM \quad (1)$$

where N is the number of earthquakes with magnitude greater than M occurring in a given time period. a is the intercept on the vertical axis, and it varies with the number of earthquakes in time and area sampled. b is the absolute value of the slope of the distribution, and its value is generally about 1.0 (Stein and Wyssession, 2013). The magnitudes of completeness were estimated for North America, Europe-North Africa, the

rest of the Atlantic coast of Africa, the Caribbean, South America and the MAR as 3.5, 3.5, 4.4, 3.2, 3.5 and 4.8, respectively (Figure 1; Appendix A). The subduction zone events were included in these completeness estimates.

The orthogonal arrangement of ridge segments and transform faults along the MAR preserves the shape of continental break up (Wilson, 1965); the paths of the ridge offsets are marked by transform faults that are also called oceanic fracture zones (Blackman and Forsyth, 1992). Oceanic fracture zones are among the most noticeable attributes of ocean basins. They are created when offsets happen at the oceanic spreading centers, and over time they can extend thousands of kilometers across the entire ocean basins (White and Williams, 1986). It is assumed by this study that the ridge seismicity is a reflection of the stress changes at the ridge and that as stress changes propagates to the ACM, the effects of these stress changes along the ACM are expressed by the passive margin seismicity. To investigate this proposition, the earthquake dataset was spatially sampled using extrapolated lines parallel to the fracture zones of the Atlantic basin at every 1° of latitude from 58°N to 38°S on the Mid-Atlantic ridge onto corresponding locations on the Atlantic coasts. The spatial distribution of earthquakes along the Mid-Atlantic ridge and the corresponding areas on the Atlantic coasts were subdivided into data bins defined by the fracture lines bounding each bin to the north and south (Figure 4).

4. Spatial Analysis

The spatial distribution of earthquakes from 1973 until 2011 along the Mid-Atlantic ridge and corresponding areas on the Atlantic margins were subdivided into bins defined by the fracture parallel lines bounding each bin to the north and south (Figure 4). The total seismic moment within each bin over the 39 year period considered was calculated by summing up the individual energy release of each earthquake event in that bin using

$$M_i = 10^{(1.5M_{wi}+16.1)} \quad (2) \quad (\text{Kanamori, 1978})$$

$$\text{Total Energy release in a bin} = \sum_{i=1}^n M_i \quad (3)$$

where n is the number of earthquakes in the bin and M_{wi} represents the moment magnitude for individual earthquake i . The equivalent magnitude M_E (equation 4) is defined as the magnitude that would be assigned to a bin if all its earthquakes happen at one instant in time.

For the spatial data series of equivalent magnitude versus position that were created, bins in the time series that have no earthquake in them were assigned an equivalent magnitude that is one tenth of magnitude lower than the completeness threshold for the area being considered. For example, the series of flat troughs between 39°S and 11°N on Figure 5 (middle diagram) represents the empty data bins along the coast of Africa with equivalent magnitude less than the completeness threshold ($mb = 4.4$) of the catalog for the Atlantic coast of Africa. The spatial bins for the African ACM which had no earthquakes in the earthquake catalog were each assigned an equivalent

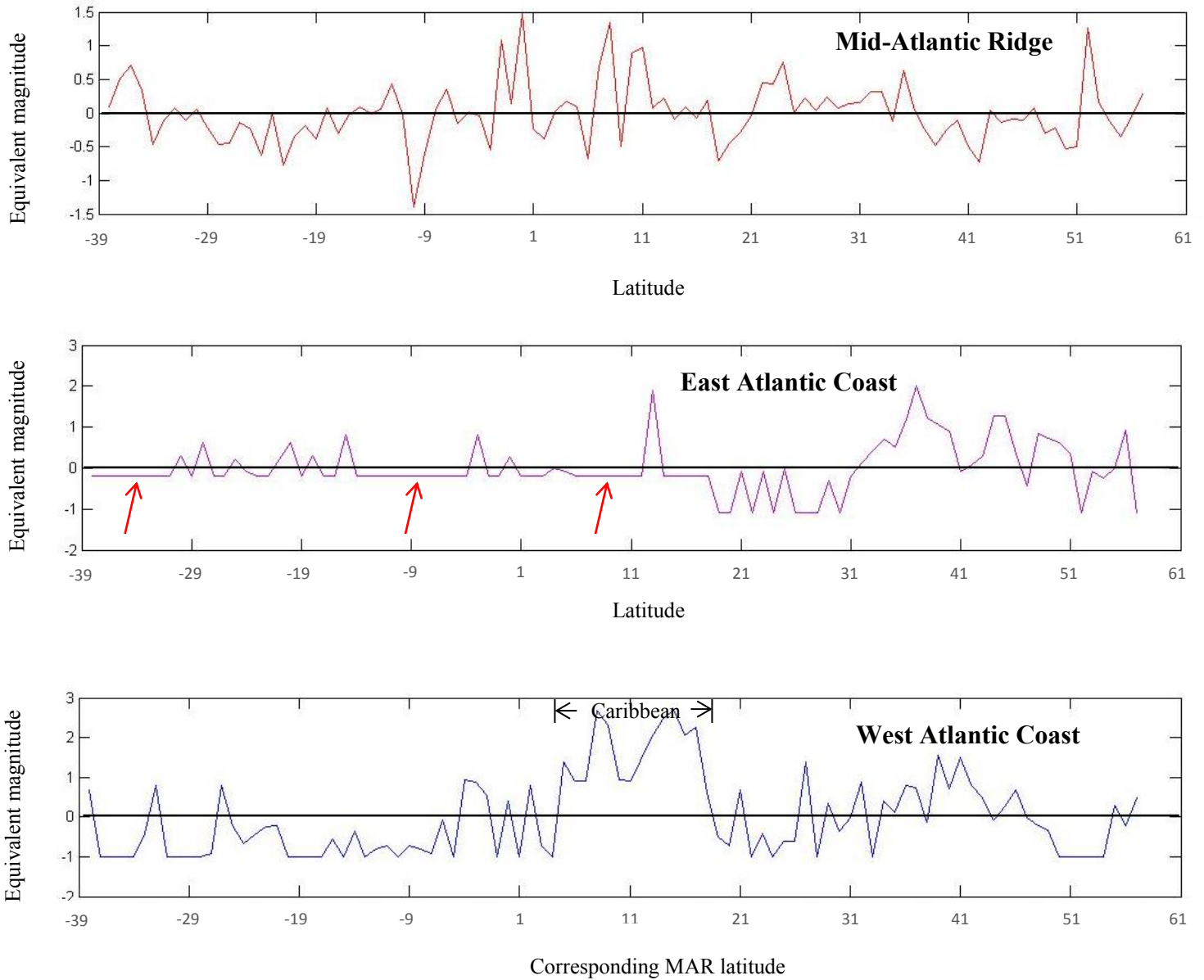


Figure 5: Plots of equivalent magnitudes against position for the MAR, East ACM and West ACM after the mean of the series has been subtracted from each data point. The red arrows in the middle diagram show spatial bins for the African ACM which had no earthquakes in the earthquake catalog. The completeness threshold of the African ACM area is 4.4 while each spatial bin with no earthquake was assigned an equivalent magnitude that is one-tenth unit less that the completeness threshold of the data set (i.e., a magnitude of 4.3). The Europe-North Africa segment of the plot has a completeness threshold of 3.5.

magnitude of 4.3, which is a tenth order of magnitude less than the catalog's completeness threshold of 4.4.

The body wave magnitude saturates above about magnitude 7 (Cosentino et al., 1977; Berril and Davis, 1980). Since all but four earthquakes in the catalogs used have magnitudes equal to or below a body-wave magnitude of 7, the body-wave magnitudes of all events used for this study were equated to the moment magnitude M_w and the seismic moment was calculated using Equation (2). The total seismic moment per bin was rescaled using Equation (4) to

$$M_E = \frac{2}{3} \left[\log \left(\sum M_i \right) - 16.1 \right] \quad (4).$$

The equivalent magnitude M_E is defined as the magnitude that would be assigned to a bin if all its earthquakes happen at one instant in time. The mean value of the equivalent magnitude spatial series was subtracted from each data point of the signal, with the resulting signal called here the residual equivalent magnitude signal.

The spatial series of residual equivalent magnitudes at the MAR was correlated with the spatial series of residual equivalent magnitudes along the west and east ACM. Normalized cross-correlations were used for all signals analyzed in this study such that each cross-correlation signal is normalized by the square root of its energy. Each spatial cross-correlation signal was tested for randomness as the correlation coefficients values obtained from cross-correlating pairs of spatial series were compared with the correlation coefficients that result from cross-correlating random signals generated using the same statistical properties of the actual spatial series. Each simulated random signal was made using the same mean, standard deviation and signal length as that of the actual spatial

series (Schilling and Harris, 2012). Equivalent magnitudes were randomly distributed on the MAR, the Atlantic basin and the ACM, and cross-correlations of these random, uncorrelated synthetic dataset were done 200 times. The cross-correlation results from the actual data were compared with those from the random signals to determine if any of the coefficients in the cross-correlations of the actual signals exceed those of the random signals.

The peak negative correlation coefficient of -0.39 observed at a spatial shift of 5° from correlating the entire MAR and east ACM seismicity is greater than all the maximum correlation coefficients obtained from cross-correlating the generated random signals (Table 1; Figure 6). Given the observed maximum correlation coefficients and the small shifts at which they occur, it appears that areas along the MAR with high seismicity are associated with areas with low seismicity on the east ACM. Unlike the east Atlantic margin, the cross correlation of MAR seismicity with that of west Atlantic margin has a peak negative correlation of -0.08 at spatial shift of 4° ; this correlation coefficient is less than all the maximum correlation coefficients obtained from cross-correlating the random signals (Table 1; Figure 7) and indicates no correlation of the MAR seismicity with that of the west Atlantic margin.

The spatial series of equivalent magnitude distribution between latitudes 19°N and 58°N on the North MAR was correlated with that along corresponding segment on the Europe-North Africa coast (Figure 8). The cross-correlation signal in Figure 8 reveals a cluster of rather large negative correlation coefficients at spatial shifts of up to 6° , with the greatest correlation value of -0.59 at a shift of 5 deg. The maximum correlation coefficient value is larger than the maximum negative correlation coefficient of -0.54

Table 1: Cross-correlation results obtained from correlating random signals having the same statistical properties as the MAR and the ACM equivalent magnitude signals.

Spatial Correlation of:	Highest of the set of maximum negative correlation coefficients	Percentage of maximum negative correlation coefficients of random signals greater than the maximum negative correlation coefficient of the real signal
MAR with entire west ACM	-0.3448	100
MAR with entire east ACM	-0.3242	0
North MAR with North America Atlantic coast	-0.4675	5
North MAR with Europe-North Africa	-0.5446	0

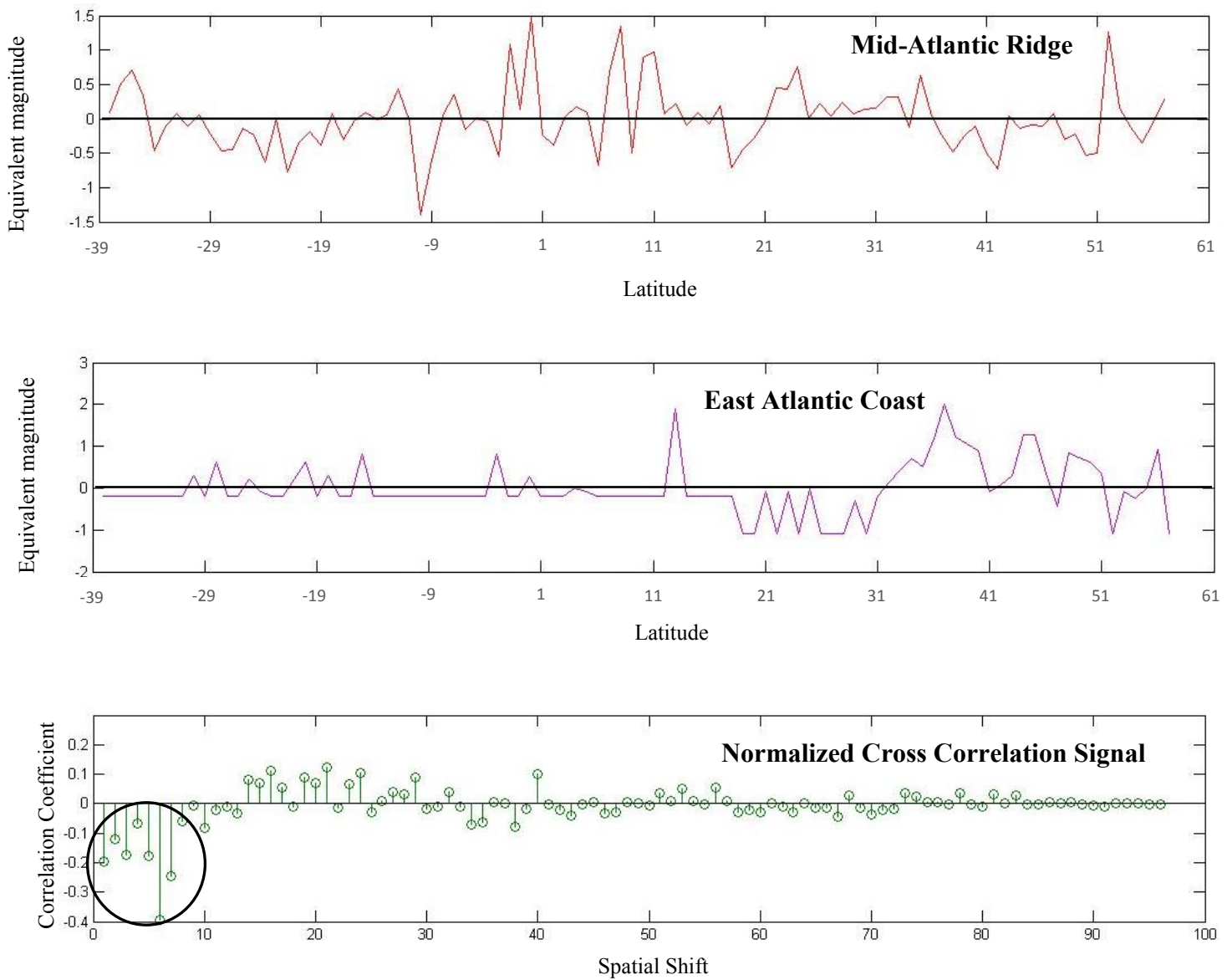


Figure 6: Cross correlation of deviation of equivalent magnitude for the MAR with that of East Atlantic coast. The circled data points show the cross-correlation coefficients discussed in the text.

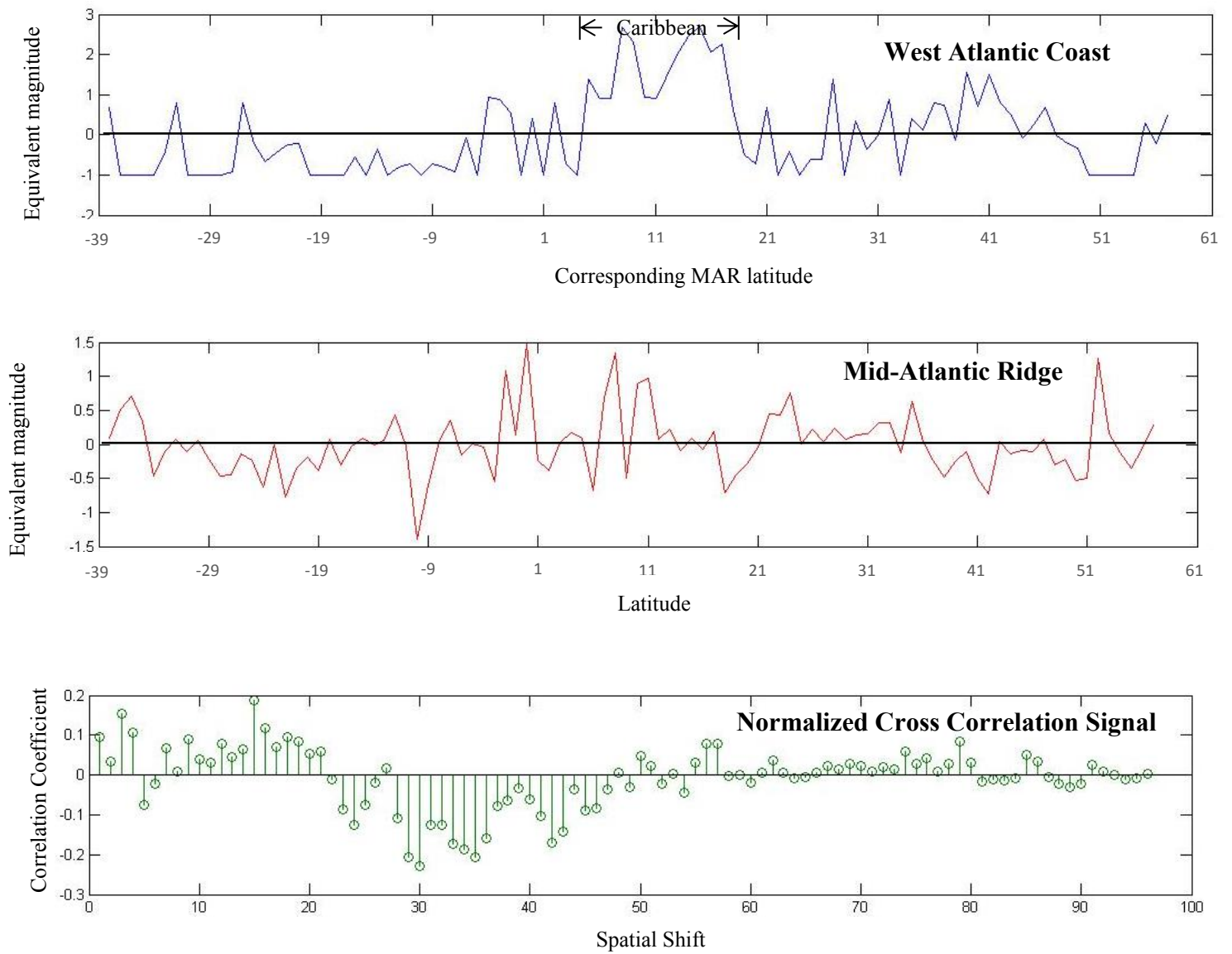


Figure 7: Cross correlation of deviation of equivalent magnitude for the MAR with that of West Atlantic coast.

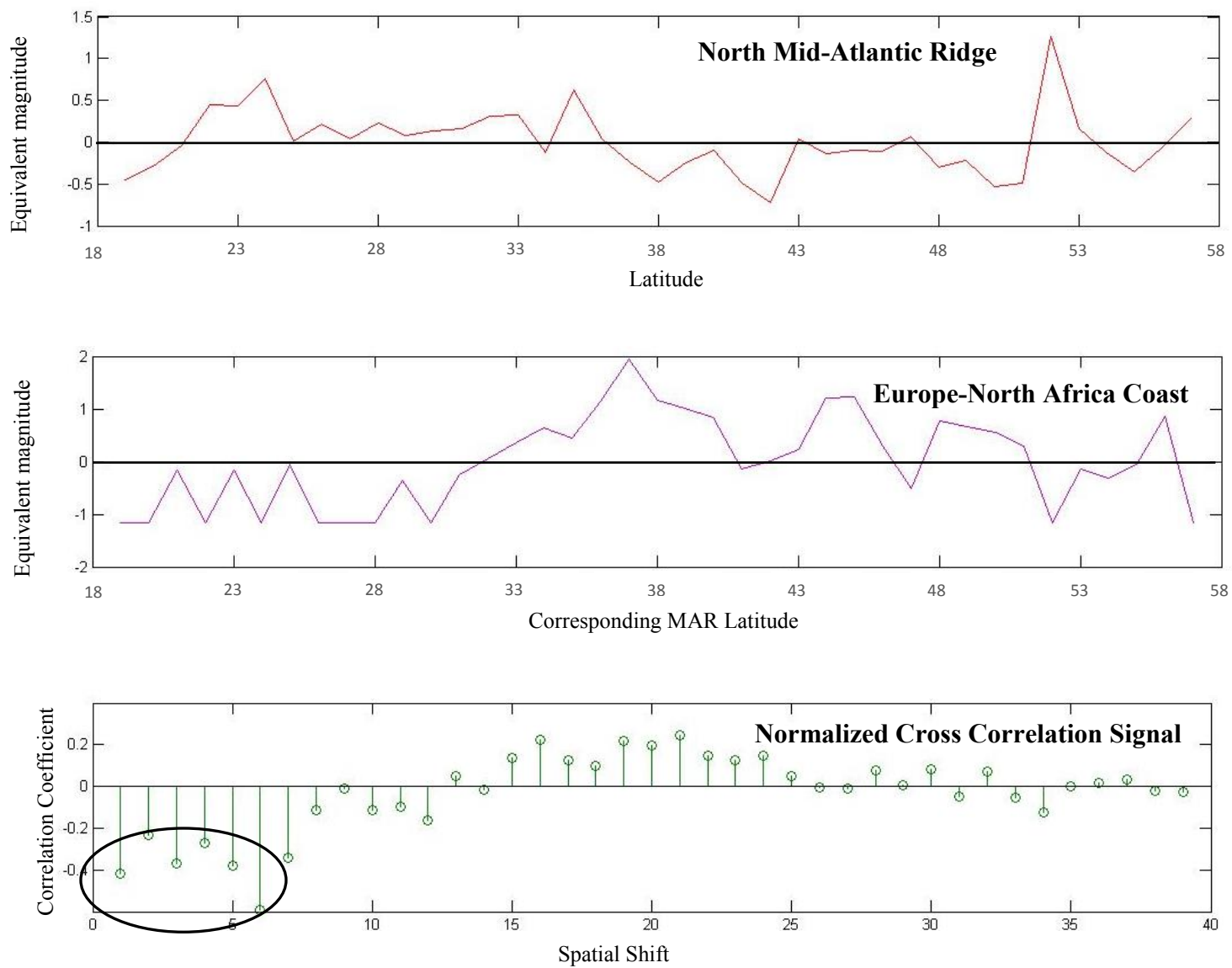


Figure 8: Cross correlation of deviation of equivalent magnitude for the North MAR with that of Europe-North Africa Coast. The circled data points show the cross-correlation coefficients discussed in the text.

generated from the correlations of the 200 random noise signals (Table 1). This suggests a low probability that random signals have a correlation value as negative as -0.59. Similarly, correlation between the distribution of equivalent magnitudes along the north MAR and corresponding segments of the North America coast shows a cluster of negative correlation coefficients at smaller spatial shift values up to 5° (Figure 9). The distribution of the maximum negative correlation coefficient obtained from the synthesized random noise series shows that only 5% of the maximum negative correlation coefficients of the random signals are greater than the maximum negative correlation coefficient of -0.41 that was generated from correlating the real signals (Table 1). Therefore, the most negative correlation value from the actual data has about a 5% chance (10 out of 200) of occurring by random chance. The occurrence of these significant anticorrelations at small spatial shifts suggests that areas on the North MAR with high equivalent magnitude appear to be associated with areas with relatively lower equivalent magnitude on both sides of the North Atlantic coast and vice versa.

In the North Atlantic section of the study area, it seems that areas on the north MAR with high seismicity spatially correspond to areas with relatively lower seismicity on both sides of the Atlantic coasts and vice versa. Similarly, areas on the whole stretch of the MAR with high seismicity spatially correspond to the entire east ACM segments with lower seismicity; however, there seems to be no significant association between the distribution of MAR seismicity and that along the west ACM.

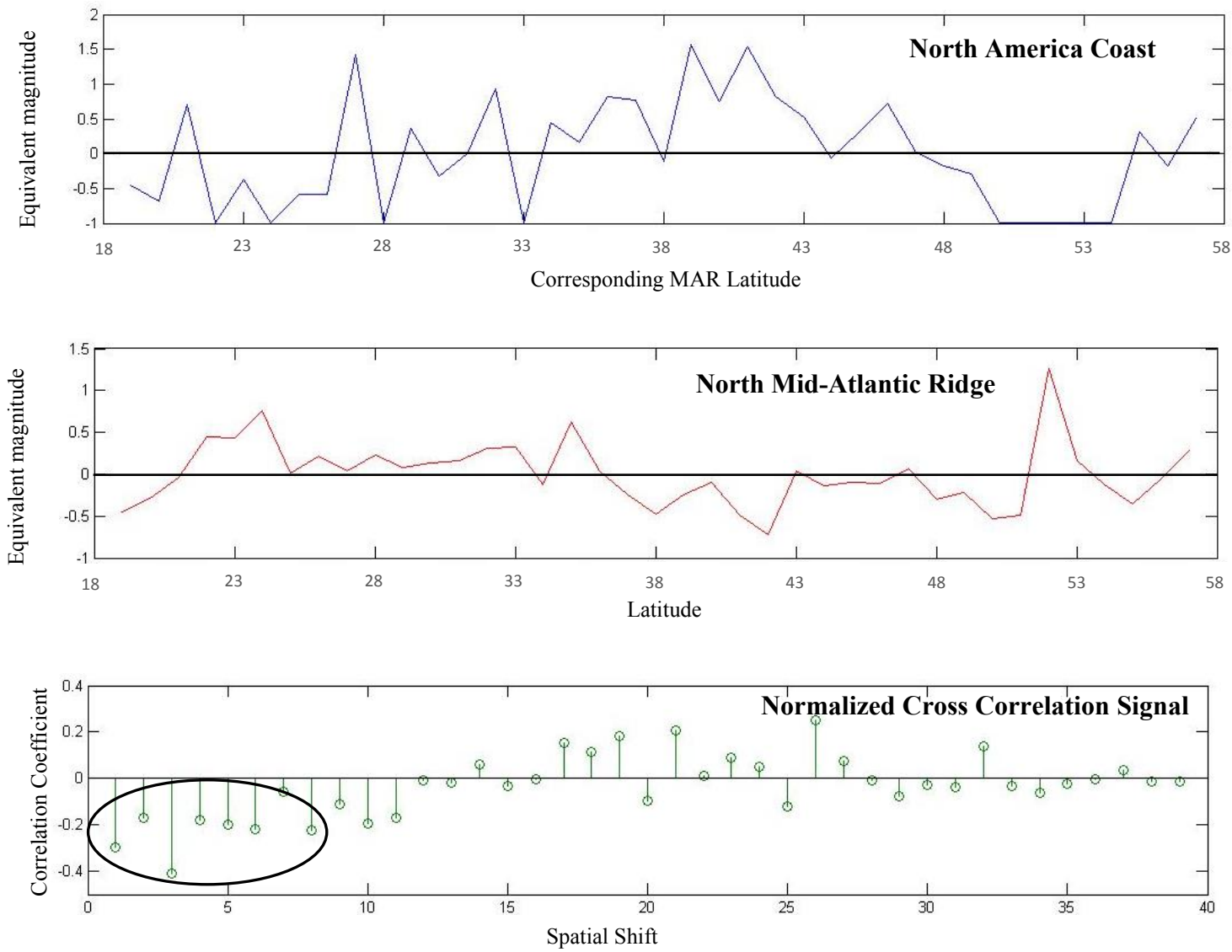


Figure 9: Cross correlation of deviation of equivalent magnitude for the North MAR with that of North America Coast. The circled data points show the cross-correlation coefficients discussed in the text.

5. Temporal Analysis

5.1 Temporal Analysis Procedure and Result

Latchman (2011) observed that magnitude 6 and greater earthquakes at the MAR were followed by moderate to strong earthquakes 2000 *km* away near the Island of Tobago with a uniform delay of 36 ± 4 *months*. This phenomenon observed by Latchman (2011) is explored in this thesis to see if it is also found to occur in other parts of the MAR and Atlantic margins. The analysis employed here is based on the solution to the Elsasser (1969) stress diffusion model. Given a tectonic plate with thickness h_1 and Young's modulus E underlain by a viscous asthenosphere of thickness h_2 and viscosity η , the stress diffusion equation is expressed as:

$$\frac{\partial u}{\partial t} = K \left(\frac{\partial^2 u}{\partial x^2} \right) \quad (5);$$

where $K = \frac{h_1 h_2 E}{\eta}$ (Elsasser, 1969).

The standard solution of the stress diffusion equation is given by

$$x = (4Kt)^{\frac{1}{2}} \quad (6)$$

where x is the mean distance travelled by a propagating stress front over a period of time t .

From Latchman's observations at Tobago, $x = 2000$ *km* and $t = 39 \pm 4$ *months*. Using the upper and lower limits of t from her observations (i.e., $t_{max} = 43$ *months* and $t_{min} = 35$ *months*) and the value of x of 2000 *km* in equation 6 above,

two K values (K_{max} and K_{min}) were calculated. The K values were each used in equation 6 to predict the range of time that earthquake(s) might be expected to occur at different points away from the MAR given that a magnitude 6 or greater earthquake had occurred at the MAR. For the purpose of this study, this time range will be referred to as Latchman's time range.

As explained earlier, the plate boundary stress path away from the MAR varies from the north Atlantic to the central Atlantic and to the south Atlantic (Figure 3). The maximum difference in latitude between the location of the stress trajectory on the MAR and the latitude of a point on the ACM on that same stress trajectory is 7.1° . Some physical area away from an MAR earthquake must be defined to test Latchman's observation in other areas of the Atlantic. Therefore, for each MAR earthquake with magnitude 6 or greater, the associated oceanic and continental margin earthquakes that fall within Latchman's time range were analyzed within an area that spans 7° north and 7° south of the latitude of the epicenter of the MAR earthquake being considered, and this area is bounded to the north and south by the extension of the fracture line zones to the Atlantic margins as illustrated in Figure 10.

To determine if the occurrences of earthquakes away from the MAR are correlated according following Latchman's model, earthquake rates of the Atlantic basin and margin earthquakes that are spatially related to each magnitude 6 or greater MAR earthquake are calculated and compared to a synthetic earthquake rate. That synthetic earthquake rate is generated for the same spatial area for Atlantic basin and margin earthquakes using a Poisson model. For each magnitude 6 and greater MAR earthquake, the number of ACM earthquakes that are spatially associated (Figure 10) with the MAR

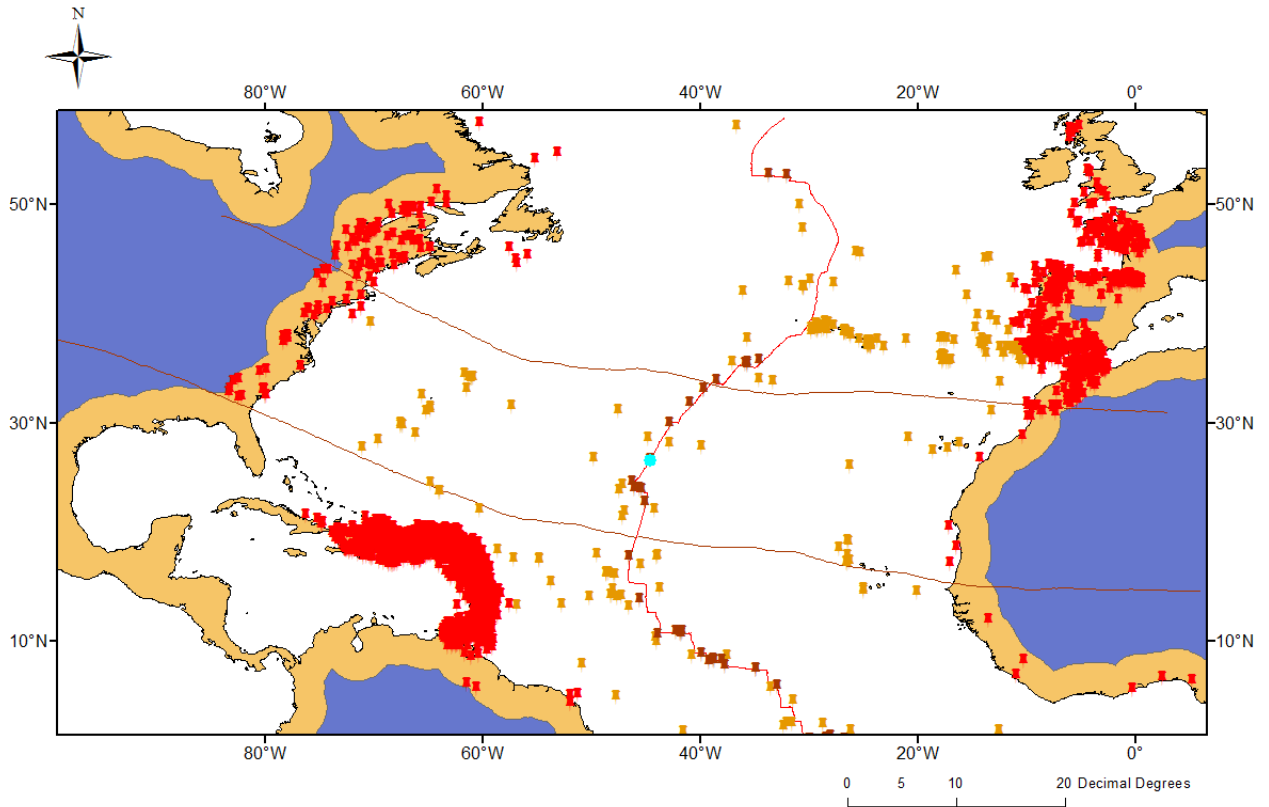


Figure 10: An illustration of how Latchman’s observation and the stress diffusion model were applied to the study area. A MAR earthquake (in light green) with fracture lines extrapolated from the MAR 7° north and south of the earthquake’s epicenter to the Atlantic margins is shown. The fracture lines are the northward and southward limits of the area within which the stress changes from the MAR earthquake in light green is proposed to influence seismicity away from the MAR axis.

event in question was recorded. The observed earthquake count was divided by the 39-year period over which the dataset spans to calculate the expected value of earthquake rate for the area defined (Figure 10). For instance, there are 315 ACM earthquakes that are spatially associated with the one MAR event that was considered, and therefore the expected earthquake rate (per year) of the associated ACM events is 315 earthquakes/39 years, which is 8.08 earthquakes/year.

The observed earthquake rates are computed in units of number of earthquakes/8 months since the Latchman time window that was adopted for this analysis is an 8-month period (± 4 months). The units of the observed earthquake rates were scaled up by a factor of three-halves ($3/2$) to convert the unit of earthquake rate from earthquake count/8 months to earthquake counts/year.

To quantify the level of significance of the difference between the observed and calculated Poissonian earthquake rates, a statistical hypothesis test was carried out to ascertain whether the mean of the observed margin earthquake rates is significantly greater than the mean of the calculated average margin earthquake rate. The null hypothesis of the statistical test is that there is no difference between the observed margin earthquake rate and the earthquake rate generated from the Poisson model. The alternative hypothesis is that the observed earthquake rate is significantly greater than the calculated earthquake rate from the Poisson model. The p-value of the distribution of difference between the observed and the synthetic rates was calculated to affirm or reject the null hypothesis. The hypothesis test result revealed a p-value of 0.1562, which suggests that the null hypothesis cannot be rejected at a 90% confidence level.

The distribution of differences between observed and calculated average margin earthquake rates that fall within Latchman's time range is displayed in Figure 11. As can be seen from Figure 11, most of the rate differences are distributed around a difference of zero between the two distributions of means. This further buttresses the statistical test result that there is likely no statistically significant difference between the observed mean earthquake rate of 36.7 events/year and the mean of the average rate (23.6 events/year) calculated from the Poisson probability distribution (Appendix C) for the Atlantic margin regions.

The same test used for the Atlantic margin regions was also applied to the oceanic crust between the MAR and the ACM regions. For this test also, the distribution of differences between observed oceanic event rate and calculated average oceanic event rate reveal that most of the rate differences are distributed around the zero difference mark (Figure 12). The mean of the observed oceanic event rate (0.63 events/year) is less than the mean of the expected event rates (0.97 events/year) from the Poisson probability model (Appendix C).

From the histograms and the outcome of the hypothesis test, earthquakes do not appear to be happening more frequently away from the MAR than is expected based on a Poisson distribution model. Most of the rate differences are near a difference of zero between the distributions of observed earthquake rates and the calculated earthquake rates considered, which suggests that seismicity was just taking place randomly away from the MAR. Based on this test, it appears that the Latchman's model does not hold for other areas along the ACM.

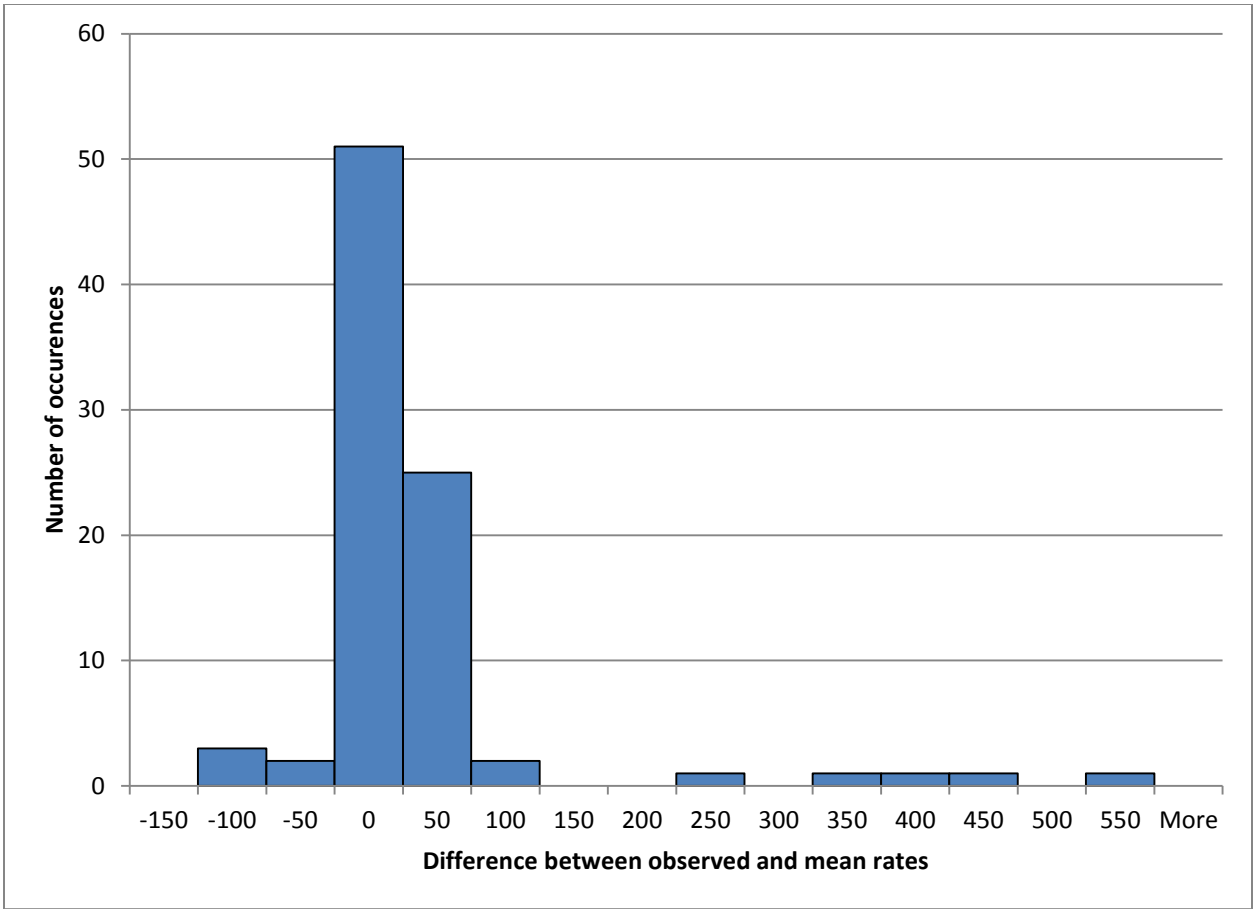


Figure 11: Distribution of the difference between the observed and mean margin earthquake rates (in units of events/year) for the ACM.

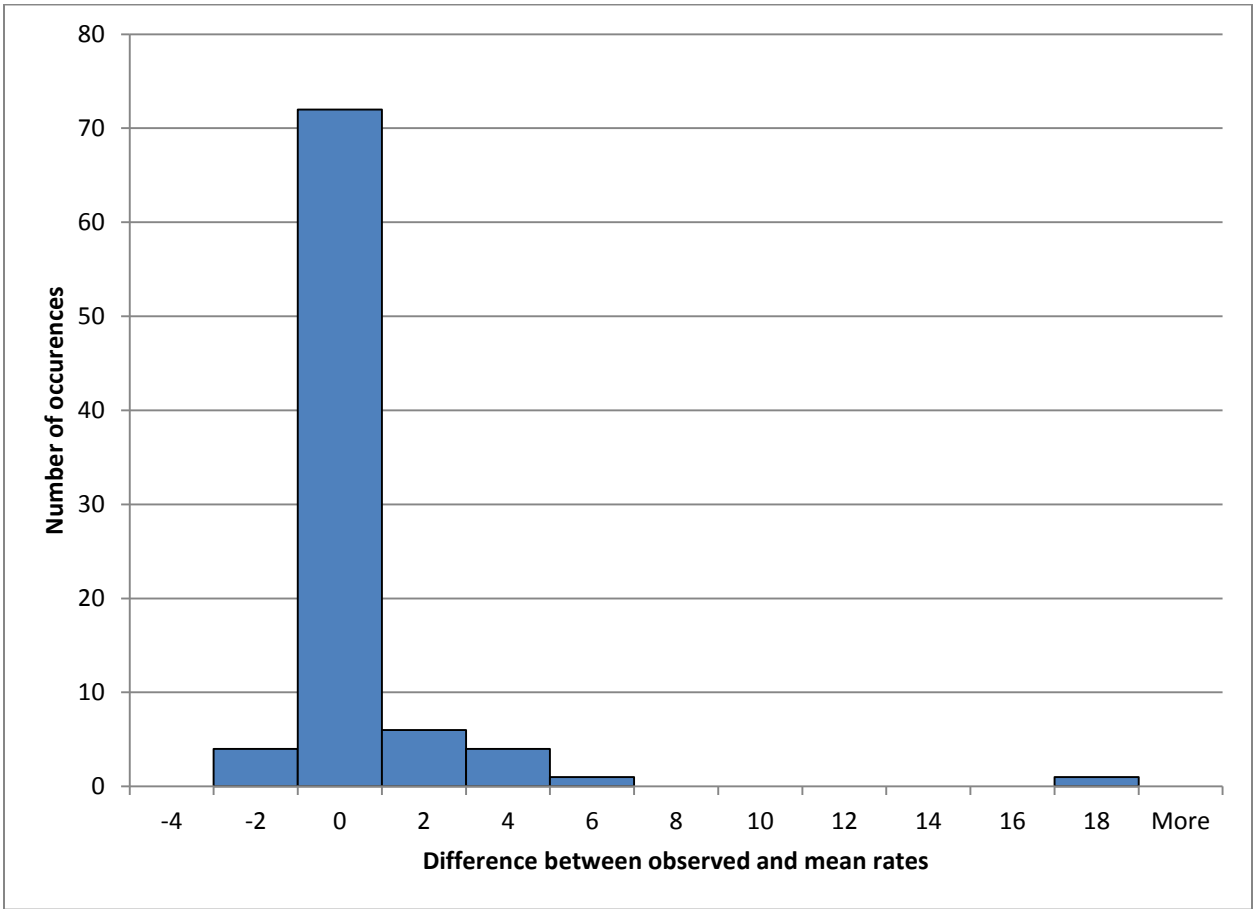


Figure 12: Distribution of the difference between the observed and mean oceanic earthquake rates (in units of events/year) for the Atlantic Basin.

6. Spatiotemporal Analysis

The orthogonal arrangement of ridge segments and transform faults of the Atlantic Ocean basin has preserved the shape of continental break up (Wilson, 1965); the paths of the ridge offsets as the continental plates have diverged are marked by oceanic fracture zones (Blackman and Forsyth, 1992). Oceanic fracture zones are among the most noticeable topographic attributes of ocean basins. They are created when offsets happen in the oceanic spreading centers, and they develop into scars that extend thousands of kilometers across entire ocean basins (White and Williams, 1986).

The boundary forces on a tectonic plate (e.g. ridge push and slab pull) should be proportional to the length of ridge, trench or transform fault (Forsyth and Uyeda, 1975). Given that the seismic moment of the largest possible earthquake that can occur along a particular oceanic ridge segment is proportional to the length of the ridge segment on which an earthquake occurs, a longer ridge segment should transmit more stress towards the passive margins when compared to a shorter ridge segment. Moreover, large earthquakes could trigger earthquakes remotely at 1000 km distance or more from its epicenter (Freed, 2005; Pollitz et al., 2012).

Given that different parts of the MAR might become seismically active at different times, a spatiotemporal analysis of the data in this thesis was carried out to investigate if local ridge earthquake activity might be associated with an increase in seismicity within the nearby ocean basin and at nearby passive margins. This analysis combines the time and spatial components of the dataset to investigate a potential relationship between MAR and ACM seismicity.

The transform faults offsetting the MAR segments were extrapolated parallel to the Atlantic fractures onto the ACM (Figure 13). The minimum time difference between earthquakes within the Atlantic basin (as well as along the Atlantic coast) and earthquakes along associated MAR axis and transform faults that bound the MAR axis in question to the north and south of the ridge axis was recorded. Since the completeness threshold magnitude of 4.4 of Africa coast is the largest completeness threshold of the entire data set, all event magnitudes less than 4.4 were removed from the dataset of other coastal regions for this analysis.

Distances of the epicenters of Atlantic basin and Atlantic coast earthquakes from the MAR axis were measured on the Google earth map where each path length (in *km*) was determined using the KML Path Measurer map application. Within each strip of the transform fault extensions from the MAR to the ACM, the minimum origin time difference (to the nearest day) between the Atlantic basin (or Atlantic coast events) and prior MAR events was recorded and plotted against the distance of each Atlantic basin/Atlantic coast earthquake from the MAR axis. For example, given an earthquake at the ACM, its origin time was compared with the origin times of all the prior earthquakes at the MAR axis as well as earthquakes within the two transform faults that bound the MAR axis to the north and south of a particular MAR segment. The prior MAR or transform event that is closest in origin time to the ACM earthquake's origin time is then selected and the difference between the two origin times was calculated and plotted against the distance of the ACM earthquake in question from the MAR axis.

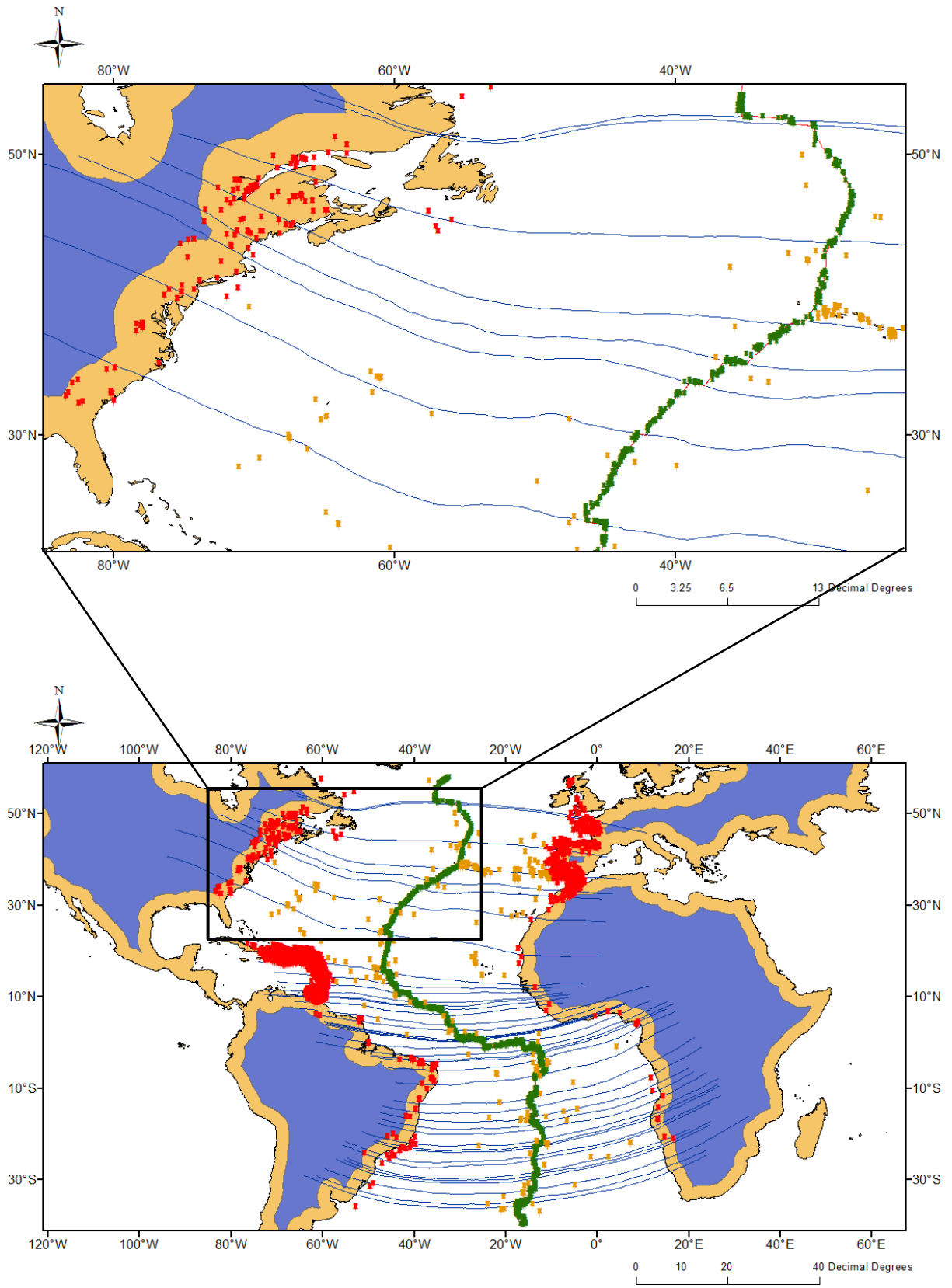


Figure 13: Study area showing the mapped transform faults of the Atlantic basin onto the Atlantic coasts. The blow-up gives a clearer view of the extension of the transform faults to the coasts.

The plot of distance of Atlantic basin event from MAR axis against difference in origin times of basin event and the corresponding prior MAR event closest in time in Figure 14 shows a trend line slope of -0.1016 with an R^2 value of 0.0514. The small, negative trend is statistically insignificant but it suggests that if there is any trend at all in the data, it is towards the ridge such that the time difference between the occurrence of prior MAR events and Atlantic Basin earthquakes is increasing towards the MAR axis and not away from the ridge as postulated by the research question for which this analysis was carried out. The extremely low R^2 value indicates that there is no linear relation between the distance of Atlantic basin event from MAR axis and time difference between the occurrence of prior MAR event and Atlantic Basin earthquakes.

Figure 15 shows the distance and time difference plot between origin times of the Atlantic coast earthquakes and prior MAR axis or transform events. The scatter plot on figure 15 shows a trend line slope of -0.081 (close to zero) and an R^2 value of 0.0295. The negative trend line indicates that the time difference between the occurrence of prior MAR event and Atlantic ACM earthquakes is increasing towards the MAR axis. These very low R^2 values indicate that there is no linear relation between the two quantities on the plot.

The analysis does not show any time-space correlation between the MAR earthquakes and either the Atlantic Basin earthquakes or the ACM earthquakes. No evidence was found to suggest the migration of seismicity away from the MAR following a large earthquake at the MAR. Therefore, it does not seem like local ridge activity is associated with an increase in seismicity within the nearby ocean basin and at nearby passive margins.

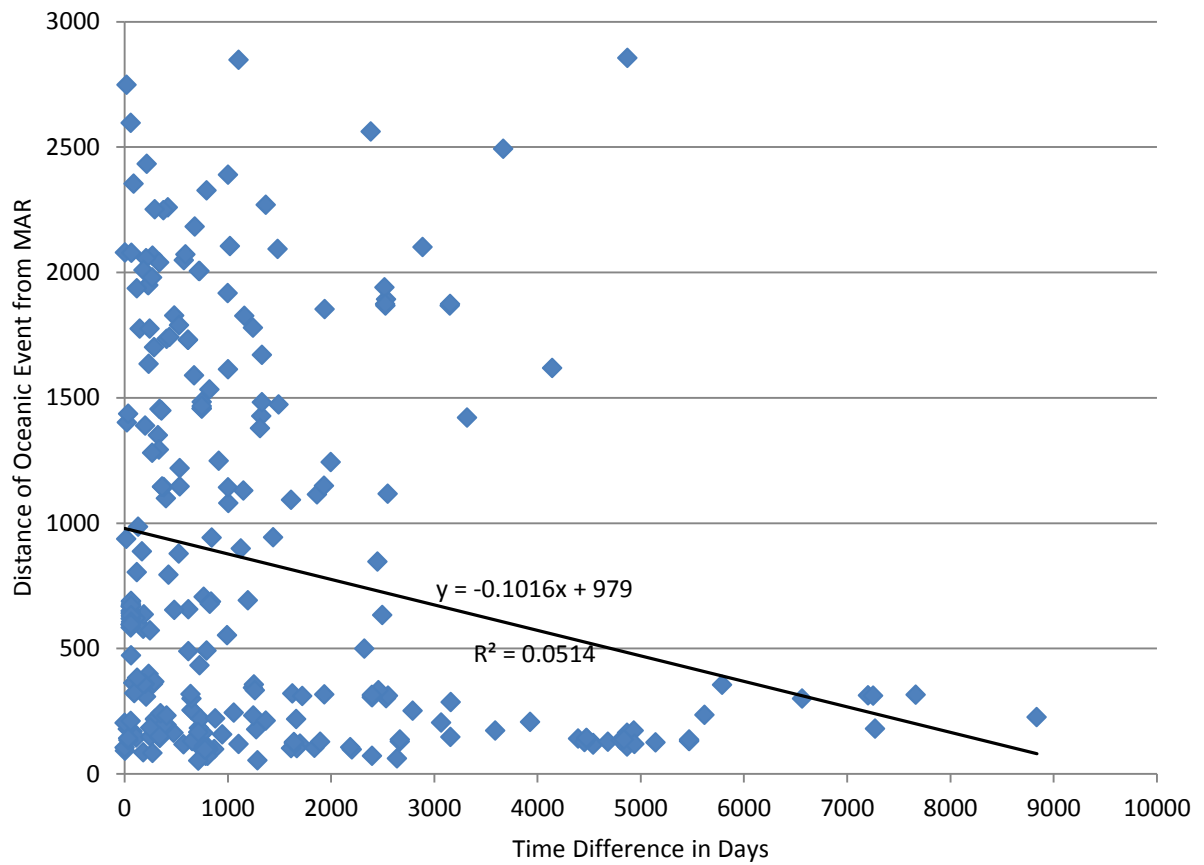


Figure 14: Plot of the distances of Atlantic basin earthquakes from the Mid-Atlantic ridge axis against time difference between the Atlantic basin event and prior MAR event closest in time to the Atlantic basin event.

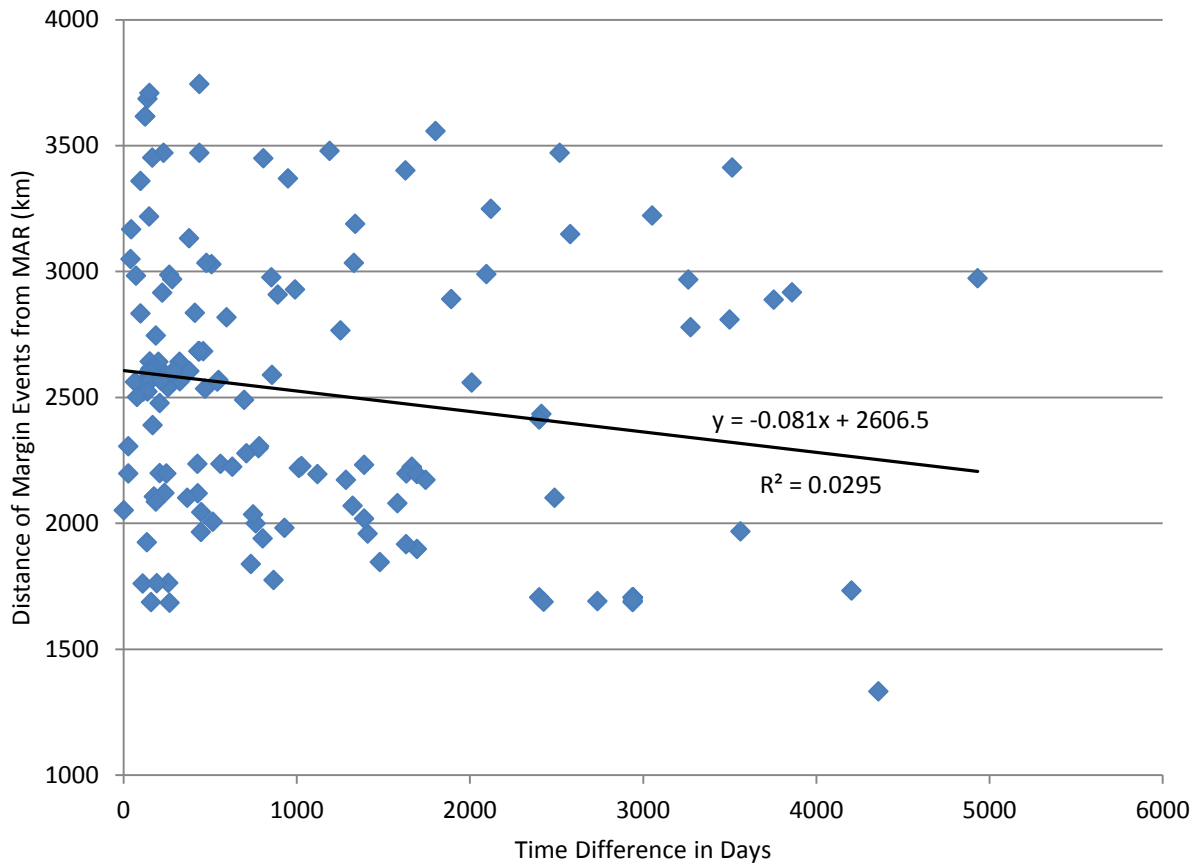


Figure 15: Plot of the distance of Atlantic coast earthquakes from the Mid-Atlantic ridge axis against time difference between the Atlantic coast event and prior MAR event closest in time to the Atlantic coast event.

7. Discussion

Three main results were found from this study. The first is the observation that areas with higher seismic moment release along the north MAR spatially correlate with areas with relatively lower seismic moment release along the north ACM and vice versa. The inverse spatial correlation observed between MAR seismicity and ACM seismicity might be due to the time (likely a long time) it takes stress changes from segments of the MAR currently experiencing high seismic activity to propagate to the associated passive margin areas presently experiencing relatively low seismic activity.

The second principal result is that the number of Atlantic basin and Atlantic coast earthquakes occurring away from the MAR is independent of the proximity of the earthquake epicenters from the MAR axis. This observation is consistent with the result of Wyssession et al. (1995), who ascribed the majority of the Atlantic basin earthquakes to identifiable tectonic features like hot spot swells, diffuse boundaries and fossil spreading ridges in the Atlantic basin. They also noted that the focal mechanisms of a few large earthquakes within the Atlantic basin indicate the release of local stress. The effect of local stress as noted by Wyssession et al. (1995) might have contributed to the independence of Atlantic basin and Atlantic coast earthquake proximity from the MAR.

The Latchman (2011) observation of strong earthquakes on a specific section of the MAR being followed by earthquakes on Trinidad and Tobago was tested on other areas of the MAR and ACM. It was found that that the temporal delay observed by Latchman does not exist for the seismicity along other areas along the MAR and ACM. Within the time window used for this study, it appears seismicity is occurring randomly in space away from the MAR.

Based on previous research, the ridge push force appears to be the primary source of stress associated with the earthquakes in the central and eastern United States (Zoback and Zoback, 1989). The stress field (orientation of the maximum principal stress) associated with earthquakes along much of western European plate also can be accounted for by the ridge push force (Golke and Coblenz, 1996). The ridge push force and collisional boundary forces at the southern Europe margin are responsible for the observed stress field along the southern Atlantic margin of southern Europe (Golke and Coblenz, 1996). However, the forces resulting from lateral density contrasts related to topographic features locally influence the intraplate stress field in the continental areas of Europe (Golke and Coblenz, 1996). The stress field along the Atlantic coast of Brazil also appears to be due to ridge push force and other plate boundary forces, compression due to lateral density variation between oceanic/continental crusts and compression due to bending of the lithosphere as a result of thick sedimentary load along the continental shelf (Assumpcao, 1998). The primary source of stress along western and southern Africa again appears to be the ridge push force (Zoback, 1992).

Golke and Coblenz (1996) estimated that the magnitude of the ridge push forces exerted on the western European plate is of the order of 20-30 MPa, and this force is responsible for the dominant NW trend of the maximum horizontal stress in that area. The magnitude of the predicted stress in southeast Europe is 12 MPa. The magnitude of the predicted stresses was observed to be reduced by lateral density variations within the continental areas of Europe (Golke and Coblenz, 1996). This horizontal stress resulting from lateral density variations throughout the lithosphere has been estimated to be in the range 10 to 100 MPa (Fleitout, 1991).

The E-W orientation and magnitude of around 25 MPa predicted for the maximum horizontal stress field within the South American plate was proposed to be due to a net torque of $6.8 \times 10^{25} Nm$ acting on the plate. This torque is solely due to the ridge push force (Coblentz and Randall, 1996). Topographic forces resulting from continental margins and elevated continental lithosphere significantly influences the South American intraplate stress field in the continental area. The introduction of topographic forces lowered the net torque acting on the plate from $6.8 \times 10^{25} Nm$ (due to the ridge push force alone) to $4.0 \times 10^{25} Nm$ (Coblentz and Randall, 1996).

Richardson and Reding (1991) found that ridge forces account for the dominant ENE orientation of maximum compression throughout much of the North American plate to the east of the Rocky Mountains. Given a 50-km thick plate, the ridge-push forces are equivalent to stresses of magnitudes 40-60 MPa. The source of stress along western and southern Africa is mainly due to the ridge push force (Zoback, 1992); the magnitude of the ridge push force is widely agreed to be 2 to $3 \times 10^{12} N$ per meter of ridge length (Parsons and Richter, 1980).

The weak anticorrelations between ACM and MAR seismicity show that the ridge push force probably has some level of influence on the ACM seismicity. However, as revealed from previous research on the study area, the forces resulting from lateral density contrasts related to topographic features and lateral density variations between oceanic and continental crust also significantly influence the seismicity of the Atlantic coastal margins.

8. Conclusion

This study investigated the relationship between MAR and ACM seismicity by testing if:

- (1) local earthquake rates are proportional to local stress changes at the MAR.
- (2) there is an observable time delay between MAR seismicity and earthquakes along the ACM.
- (3) earthquakes closer to the MAR axis happen earlier relative to the events happening farther away from the MAR.

To test these hypotheses, spatial, temporal and spatiotemporal analyses were carried out using earthquake catalogs that reported the seismicity of the study area from 1973 until 2011.

The results of the analyses lead to the following conclusions:

- (1) Within the time window (and magnitude range) of the dataset used for this study, it appears that seismicity is happening randomly in space away from the MAR; areas closer to the MAR do not experience increased seismicity when compared to areas farther away from the MAR.
- (2) The ridge push force may have some level of influence on the seismicity of the ACM, but the ridge force probably acts at the ACM along with other local forces, such as forces due to lateral density variation within the lithospheric plates.

References

- Amato, A., Montone, P., & Cesaro, M. (1995). State of stress in Southern Italy from borehole breakout and focal mechanism data. *Geophysical Research Letters*, 22(23), 3119-3122.
- Aslanian, D., Moulin, M., Olivet, J. L., Unternehr, P., Matias, L., Bache, F., Rabineau, M., Nouzé, H., Frauke Klingelheofer, F., Contrucc, I., & Labails, C. (2009). Brazilian and African passive margins of the Central Segment of the South Atlantic Ocean: Kinematic constraints. *Tectonophysics*, 468(1), 98-112.
- Assumpcao, M. (1998) Seismicity and stress in the Brazilian passive margin. *Bulletin of the Seismological Society of America*, **88**, 160-169.
- Assumpcao, M., Dourado, J. C., Ribotta, L. C., Mohriak, W. U., Fabio L. D. and Barbosa, J. R. (2011). The Sao Vicente earthquake of 2008 April and seismicity in the continental shelf off SE Brazil: further evidence for flexural stresses. *Geophys. J. Int.* (2011) **187**, 1076–1088.
- Attewell, P. B., & Farmer, I. W. (1973, January). Fatigue behaviour of rock. In *International Journal of Rock Mechanics and Mining Sciences & Geomechanics Abstracts* (Vol. 10, No. 1, pp. 1-9). Pergamon.
- Ayele, A. (2002). Active compressional tectonics in central Africa and implications for plate tectonic models: evidence from fault mechanism studies of the 1998 earthquakes in the Congo Basin. *Journal of African Earth Sciences* **35** (2002), 45-50.

- Barros, L.V., Assumpcao, M., Quintero, R., and Caixeta, D.F. (2009). Intraplate seismicity in Brazil, the case of Porto dos Gaúchos seismic zone in the Amazon Craton – Brazil, *Tectonophysics*, (Amsterdam), **469**, 37-47.
- Bercovici, D. and Ricard, Y. (2000). The relationship between mantle dynamics and plate tectonics: a primer. *The History and Dynamics of Global Plate Motions*, *Geophysical Monograph 121*, M. Richards, R. Gordon and R. van der Hilst, eds., American Geophysical Union, p. 5-46.
- Berrill, J. B., & Davis, R. O. (1980). Maximum entropy and the magnitude distribution. *Bulletin of the Seismological Society of America*, *70*(5), 1823-1831.
- Bird, P., Ben-Avraham, Z., Schubert, G., Andreoli, M., & Viola, G. (2006). Patterns of stress and strain rate in southern Africa. *Journal of Geophysical Research: Solid Earth (1978–2012)*, *111*(B8).
- Blackman, D. K., & Forsyth, D. W. (1992). The effects of plate thickening on three-dimensional, passive flow of the mantle beneath mid-ocean ridges. *Geophysical Monograph Series*, *71*, 311-326.
- Bott, H.P. (1982) Stress Based Tectonic Mechanisms at Passive Continental Margins. *Dynamics of passive margins*, pp. 147-153.
- Coblentz D. D., and Richardson, R. M. (1996) Analysis of the South American intraplate stress field, *J. Geophys. Res.*, *101*(B4), 8643 – 8657.
- Coblentz, D. D., Zhou, S., Hillis, R. R., Richardson, R. M., & Sandiford, M. (1998). Topography, boundary forces, and the Indo-Australian intraplate stress

- field. *Journal of Geophysical Research: Solid Earth (1978–2012)*, 103(B1), 919-931.
- Conrad, C. (2013). Earthquake Seismology.
[http://www.soest.hawaii.edu/GG/FACULTY/conrad/
classes/GG304_S13/lectures/Lecture_22.pdf](http://www.soest.hawaii.edu/GG/FACULTY/conrad/classes/GG304_S13/lectures/Lecture_22.pdf)
- Cosentino, P., Ficarra, V., & Luzio, D. (1977). Truncated exponential frequency-magnitude relationship in earthquake statistics. *Bulletin of the Seismological Society of America*, 67(6), 1615-1623.
- DeMets, C., Jansma, P. E., Mattioli, G. S., Dixon, T. H., Farina, F., Bilham, R., Calais, E., & Mann, P. (2000). GPS geodetic constraints on Caribbean-North America plate motion. *Geophysical Research Letters*, 27(3), 437-440.
- Doré, A. G., Lundin, E. R., Kuszniir, N. J., & Pascal, C. (2008). Potential mechanisms for the genesis of Cenozoic domal structures on the NE Atlantic margin: pros, cons and some new ideas. *Geological Society, London, Special Publications*, 306(1), 1-26.
- Eagles, G. (2007). New angles on South Atlantic opening. *Geophysical Journal International*, 168(1), 353-361.
- Elsasser, W. M. (1969), Convection and stress propagation in the upper mantle, in *The Application of Modern Physics to the Earth and Planetary Interiors*, pp. 223–246, John Wiley, Hoboken, N. J.
- Emery, K. O. (1980). Continental margins--Classification and petroleum prospects.

- AAPG Bulletin*, 64(3), 297-315.
- Fejerskov, M., & Lindholm, C. (2000). Crustal stress in and around Norway: an evaluation of stress-generating mechanisms. *Geological Society, London, Special Publications*, 167(1), 451-467.
- Fleitout, L. (1991). The sources of lithospheric tectonic stresses. *Philos. Trans. R. Soc. London*, 337: 73-81
- Forsyth, D., & Uyeda, S. (1975). On the relative importance of the driving forces of plate motion. *Geophysical Journal International*, 43(1), 163-200.
- Freed, A. M. (2005). Earthquake triggering by static, dynamic, and postseismic stress transfer. *Annu. Rev. Earth Planet. Sci.*, 33, 335-367.
- Gardner, J.K., Knopoff, L. (1974) Is the sequence of earthquakes in southern California, with aftershocks removed, Poissonian? *Bulletin of the Seismological Society of America*, Vol. 64, No. 5, pp. 1363-1367.
- Golke M. and Coblenz D. (1996) Origins of the European regional stress field, *Tectonophysics*, 266, 11 – 24.
- Gutenberg, B., & Richter, C. F. (1944). Frequency of earthquakes in California. *Bulletin of the Seismological Society of America*, 34(4), 185-188.
- Gutscher, M. A., Malod, J., Rehault, J. P., Contrucci, I., Klingelhofer, F., Mendes-Victor, L., & Spakman, W. (2002). Evidence for active subduction beneath Gibraltar. *Geology*, 30(12), 1071-1074.
- Gvirtzman, Z. (2002). Partial detachment of a lithospheric root under the southeast Carpathians: toward a better definition of the detachment concept.

- Geology*, 30(1), 51-54.
- Heidbach, O., Tingay, M., Barth, A., Reinecker, J., Kurfeß, D., and Müller, B. (2008).
The World Stress Map database release 2008 doi:10.1594/GFZ.WSM.Rel2008,
2008
- Heidbach, O., Tingay, M., Barth, A., Reinecker, J., Kurfeß, D., and Müller, B. (2010).
Global crustal stress pattern based on the World Stress Map database release
2008. *Tectonophysics*, **482** (2010), 3-15.
- Hurd, O. and Zoback, MD. (2012). Intraplate earthquakes, regional stress and fault
mechanics in the Central and Eastern US, and Southeastern Canada.
Tectonophysics, **581** (2012), 182-192.
- Johnston, A.C. (1989). The seismicity of stable continental interiors, in *Earthquakes at
North-Atlantic Passive Margins: Neotectonics and Post-glacial Rebound*, p. 299-
327, eds Gregersen, S. & Basham, P.W., Kluwer Academic, Boston, USA.
- Kanamori, H. (1978). Quantification of earthquakes. *Nature*, 271, 411-414.
- Kanamori, H., & Rivera, L. (2006). Energy partitioning during an earthquake.
Earthquakes: Radiated Energy and the Physics of Faulting, 3-13.
- Knopoff, L. (1969). Continental drift and convection. *Geophysical Monograph
Series*, 13, 683-689.
- Latchman, J. and Aspinall, W. (2011). Long-range earthquake triggering near Tobago,
West Indies: precursory indicators. Abstract: IUGG, Melbourne, Australia, 2011.
- Lillie, R. J. (1999). Whole earth geophysics. *An Introductory Textbook for Geologists*.

- Manspeizer, W. (Ed.). (2013). *Triassic-Jurassic rifting: continental breakup and the origin of the Atlantic Ocean and passive margins*. Elsevier.
- Mariucci, M. T., & Müller, B. (2003). The tectonic regime in Italy inferred from borehole breakout data. *Tectonophysics*, *361*(1), 21-35.
- Marsan, D., & Bean, C. J. (2003). Seismicity response to stress perturbations, analysed for a world-wide catalogue. *Geophysical Journal International*, *154*(1), 179-195.
- McGarr, A. (1999). On relating apparent stress to the stress causing earthquake fault slip. *Journal of Geophysical Research: Solid Earth (1978–2012)*, *104*(B2), 3003-3011.
- Melosh, H. J. (1976). Nonlinear stress propagation in the Earth's upper mantle. *J. Geophys. Res.* **81**, 5621-5632.
- Minster, J. B., & Jordan, T. H. (1978). Present-day plate motions. *Journal of Geophysical Research: Solid Earth (1978–2012)*, *83*(B11), 5331-5354.
- Morgan, W. J. (1971). Convection plumes in the lower mantle. *Nature* *230*, 559-661.
- Mukhamediev, S. A., Grachev, A. F., & Yunga, S. L. (2008). Nonstationary dynamic control of seismic activity of platform regions by mid-ocean ridges. *Izvestiya, Physics of the Solid Earth*, *44*(1), 9-17.
- Muller, B., Zoback, M. L., Fuchs, K., Mastin, L., Gregersen, S., Pavoni, N., Stephansson, O. and Ljunggren, C. (1992) Regional patterns of tectonic stress in Europe. *J. Geophys. Res.* **97**, 11783-11803.

- Parsons, B., & Richter, F. M. (1980). A relation between the driving force and geoid anomaly associated with mid-ocean ridges. *Earth and Planetary Science Letters*, 51(2), 445-450.
- Pinheiro, L. M., Wilson, R. C. L., Pena dos Reis, R., Whitmarsh, R. B., & Ribeiro, A. (1996). The western Iberia margin: a geophysical and geological overview. In *Proceedings-Ocean Drilling Program Scientific Results* (pp. 3-26). National Science Foundation.
- Pollitz, F. F., Stein, R. S., Sevilgen, V., & Bürgmann, R. (2012). The 11 April 2012 east Indian Ocean earthquake triggered large aftershocks worldwide. *Nature*, 490(7419), 250-253.
- Richardson, R. M., & Reding, L. M. (1991). North American plate dynamics. *Journal of Geophysical Research: Solid Earth (1978–2012)*, 96(B7), 12201-12223.
- Rosencrantz, E., & Mann, P. (1991). SeaMARC II mapping of transform faults in the Cayman Trough, Caribbean Sea. *Geology*, 19(7), 690-693.
- Russo, R. M., Speed, R. C., Okal, E. A., Shepherd, J. B., & Rowley, K. C. (1993). Seismicity and tectonics of the southeastern Caribbean. *Journal of Geophysical Research: Solid Earth (1978–2012)*, 98(B8), 14299-14319.
- Schilling R. J. and Harris S. L. (2012). Discrete-time systems in the time domain. *Fundamentals of Digital Signal Processing*, pp. 111.
- Scholz, C.H. (1990). *The Mechanics of Earthquakes and Faulting*: Cambridge, UK, Cambridge University Press, 439 p.

- Schorlemmer D. and Woessner J. (2008) Probability of Detecting an Earthquake. *Bulletin of the Seismological Society of America*, Vol. 98, No. 5, pp. 2103-2117.
- Serpelloni, E., Vannucci, G., Pondrelli, S., Argnani, A., Casula, G., Anzidei, M., ... & Gasperini, P. (2007). Kinematics of the Western Africa-Eurasia plate boundary from focal mechanisms and GPS data. *Geophysical Journal International*, 169(3), 1180-1200.
- Silveira, G., & Stutzmann, E. (2002). Anisotropic tomography of the Atlantic Ocean. *Physics of the Earth and Planetary Interiors*, 132(4), 237-248.
- Skordas, E., Meyer, K., Olsson, R. and Kulhánek, O. (1991). Causality between interplate (North Atlantic) and intraplate (Fennoscandia) seismicities. *Tectonophysics*, **185** (1991), 295-307.
- Smith S. W. (1997) Properties of convolution. *The Scientist and Engineer's Guide to Digital Signal Processing*, pp. 137-140.
- Smith, D. K., Escartin, J., Cannat, M., Tolstoy, M., Fox, C. G., Bohnenstiehl, D. R., & Bazin, S. (2003). Spatial and temporal distribution of seismicity along the northern Mid-Atlantic Ridge (15°–35° N). *Journal of Geophysical Research: Solid Earth (1978–2012)*, 108(B3), 2167.
- Stefanick, M., & Jurdy, D. M. (1992). Stress observations and driving force models for the South American plate. *Journal of Geophysical Research: Solid Earth (1978–2012)*, 97(B8), 11905-11913.

- Stein, S. and Wysession, M. (2003). *An Introduction to Seismology, Earthquakes and Earth Structure*, p 265, 274, 326, 334.
- Stewart R. (2005) Oceanography in the 21st Century, an online textbook.
<http://oceanworld.tamu.edu/resources/oceanography-book/coastalzone.htm>,
accessed November, 2011.
- Tackley, P. J. (2000) Self-consistent generation of tectonic plates in time-dependent, three-dimensional mantle convection simulations 1. Pseudoplastic yielding. *An Electronic Journal of the Earth Sciences*, volume 1, issue 8.
- ten Brink, U. S., & López-Venegas, A. M. (2012). Plate interaction in the NE Caribbean subduction zone from continuous GPS observations. *Geophysical Research Letters*, 39(10).
- Tesauro, M., Hollenstein, C., Egli, R., Geiger, A., & Kahle, H. G. (2006). Analysis of central western Europe deformation using GPS and seismic data. *Journal of Geodynamics*, 42(4), 194-209.
- Torsvik, T. H., Van der Voo, R., Meert, J. G., Mosar, J., & Walderhaug, H. J. (2001). Reconstructions of the continents around the North Atlantic at about the 60th parallel. *Earth and Planetary Science Letters*, 187(1), 55-69.
- Turcotte, D. L. (1982) The state of stress at passive continental margins. *Dynamics of Passive Margins*, (book) pg. 141-146.
- Turcotte, D. L., Newman, W. I., & Shcherbakov, R. (2003). Micro and macroscopic models of rock fracture. *Geophysical Journal International*, 152(3), 718-728.

- Uchupi, E. & Emery, K. O. (1991). Genetic global geomorphology: a prospectus. In: Osborne, R.H. (Ed.), *From Shoreline to Abyss: Contribution in Marine Geology in Honor of Francis Parker Shepard*. SEPM Special publication, Tulsa, Oklahoma pp. 273-290.
- White, R., & McKenzie, D. (1989). Magmatism at rift zones: the generation of volcanic continental margins and flood basalts. *Journal of Geophysical Research: Solid Earth (1978–2012)*, 94(B6), 7685-7729.
- White, R. S., & Williams, C. A. (1986). Oceanic fracture zones. *Journal of the Geological Society*, 143(5), 737-741.
- Wilson, J. T. (1965). A new class of faults and their bearing on continental drift. *Nature*, 207(4995), 343-347.
- Wilson, M. (1997). Thermal evolution of the Central Atlantic passive margins: continental break-up above a Mesozoic super-plume. *Journal of the Geological Society*, 154(3), 491-495.
- Wysession, M. E., Wilson, J., Bartkó, L., & Sakata, R. (1995). Intraplate seismicity in the Atlantic Ocean Basin: a teleseismic catalog. *Bulletin of the Seismological Society of America*, 85(3), 755-774.
- Ziegler, P. A. (1992). European Cenozoic rift system. *Tectonophysics*, 208(1), 91-111.
- Zoback, M. L. (1992a) First and second-order patterns of stress in the lithosphere: the world stress map project. *J. Geophys. Res.* **97**, 11703-11728.
- Zoback M. L. and M. Magee (1991) Stress magnitudes in the crust: Constraints from stress orientation and relative magnitude data, *Philos. Trans. R. Soc. London, Ser.*

A, 337, 181 – 194.

Zoback, M. L., & Mooney, W. D. (2003). Lithospheric buoyancy and continental intraplate stresses. *International Geology Review*, 45(2), 95-118.

Zoback, M. L., & Zoback, M. D. (1989). Tectonic stress field of the continental United States. *Geological Society of America Memoirs*, 172, 523-540.

Zoback, M. L., Zoback, M. D., Adams, J., Assumpcao, M., Bell, S., Bergman, E. A., ... & Zhizhin, M. (1989). Global patterns of tectonic stress. *Nature*, 341(6240), 291-298.

Appendix A: Supplemental figures for section 3 showing the Gutenberg-Richter plots for the different regions of the study area.

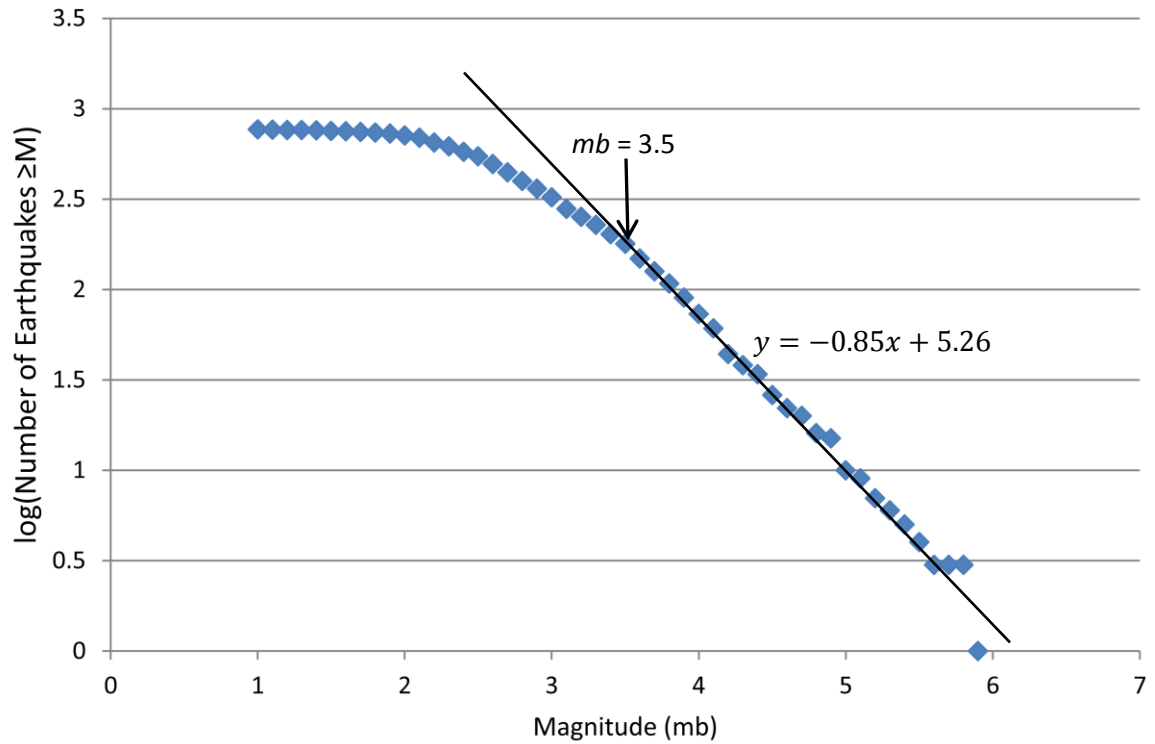


Figure A1: Gutenberg-Richter Plot for the Atlantic coast of North America. The $mb = 3.5$ point on the plot shows where the distribution deviates away from a linear trend.

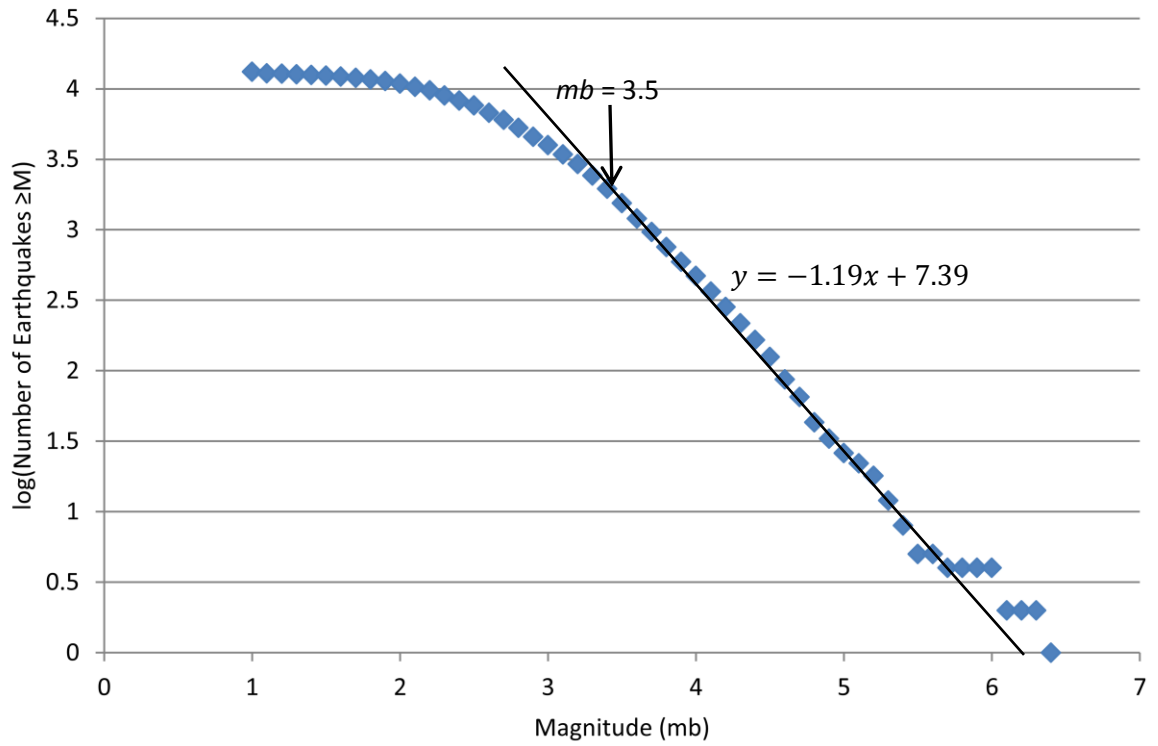


Figure A2: Gutenberg-Richter Plot for the Atlantic coast of Europe and North Africa. The $mb = 3.5$ point on the plot shows where the distribution deviates away from a linear trend.

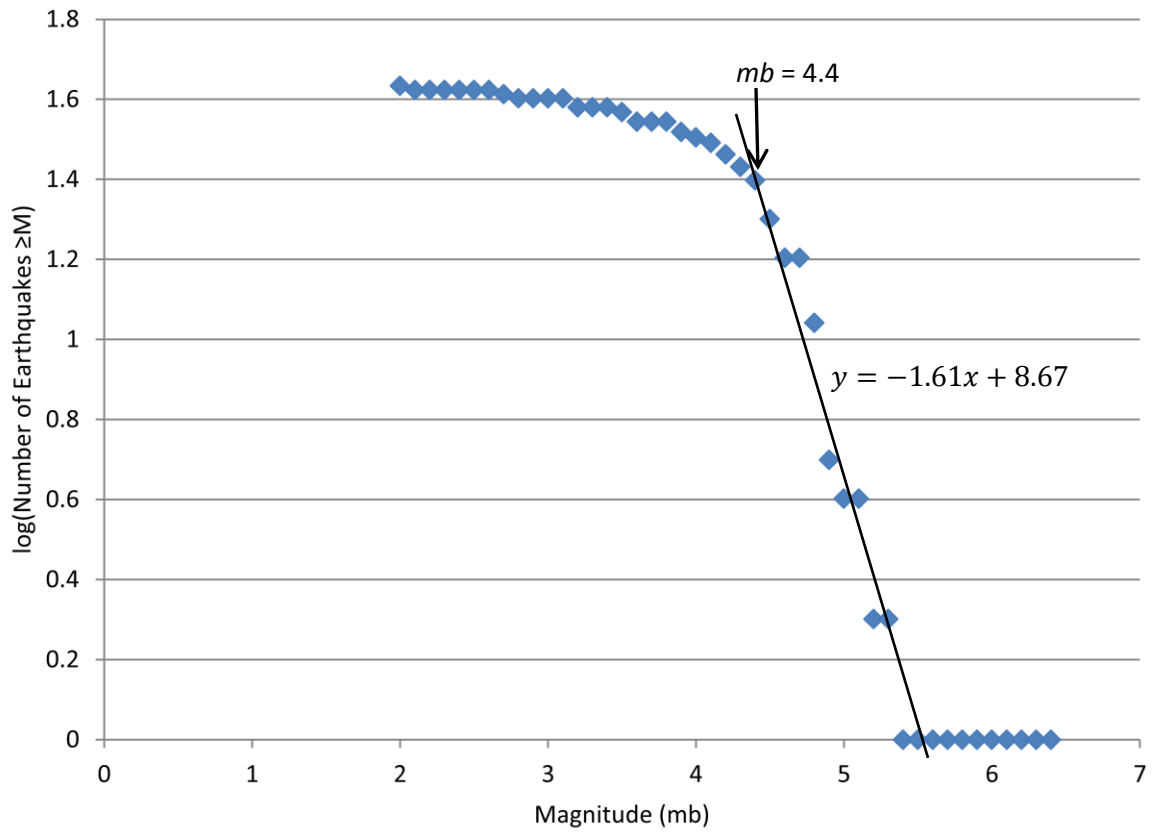


Figure A3: Gutenberg-Richter Plot for the Atlantic coast of Africa (south of 15°N). The $mb = 4.4$ point on the plot shows where the distribution deviates away from a linear trend.

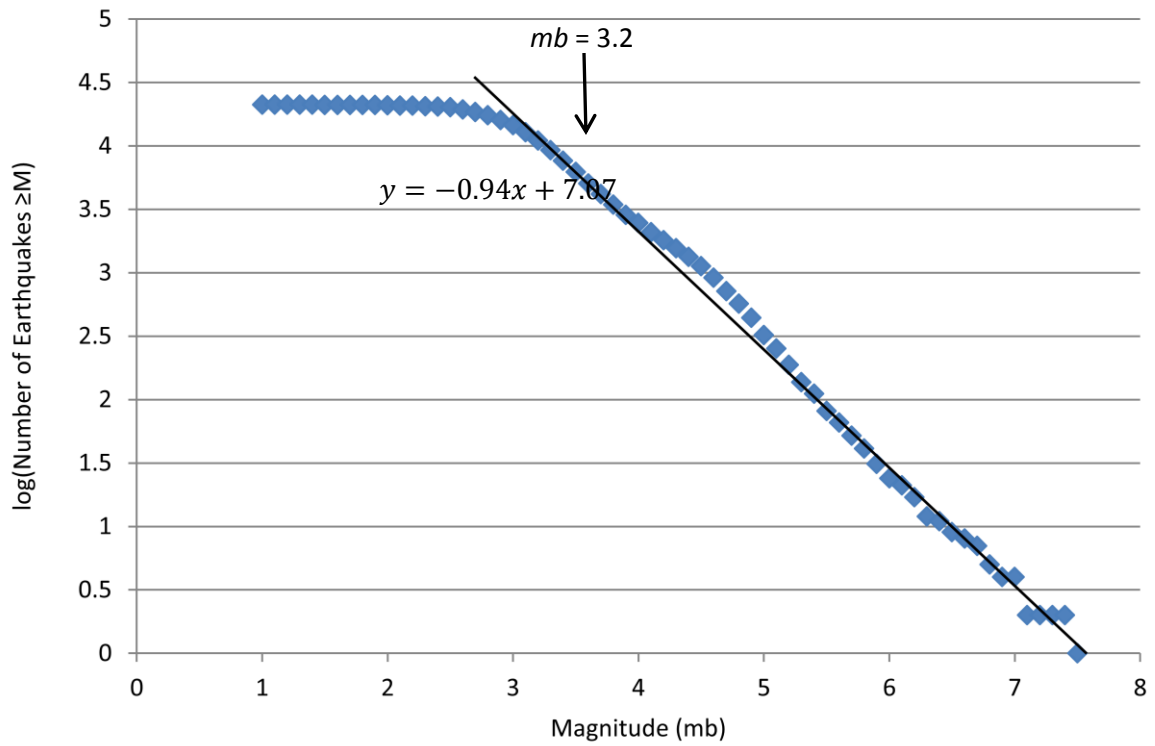


Figure A4: Gutenberg-Richter Plot for the Atlantic coast of the Caribbean. The $mb = 3.2$ point on the plot shows where the distribution deviates away from a linear trend.

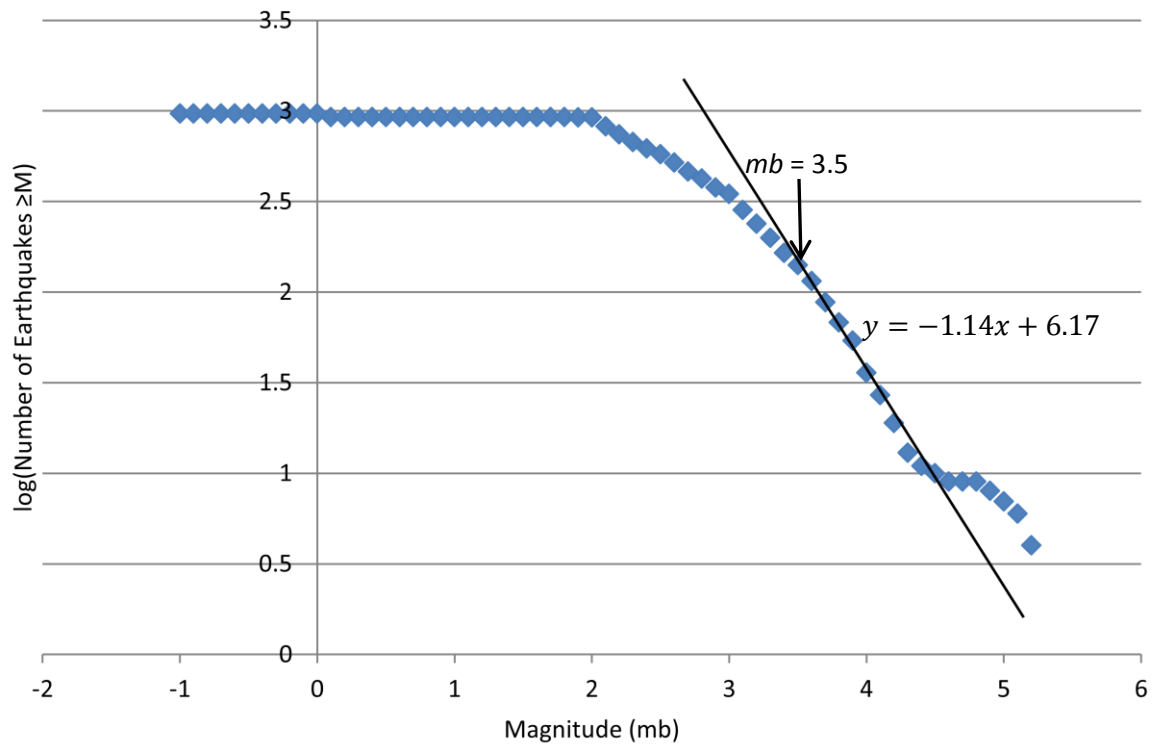


Figure A5: Gutenberg-Richter Plot for the Atlantic coast of South America. The $mb = 3.5$ point on the plot shows where the distribution deviates away from a linear trend.

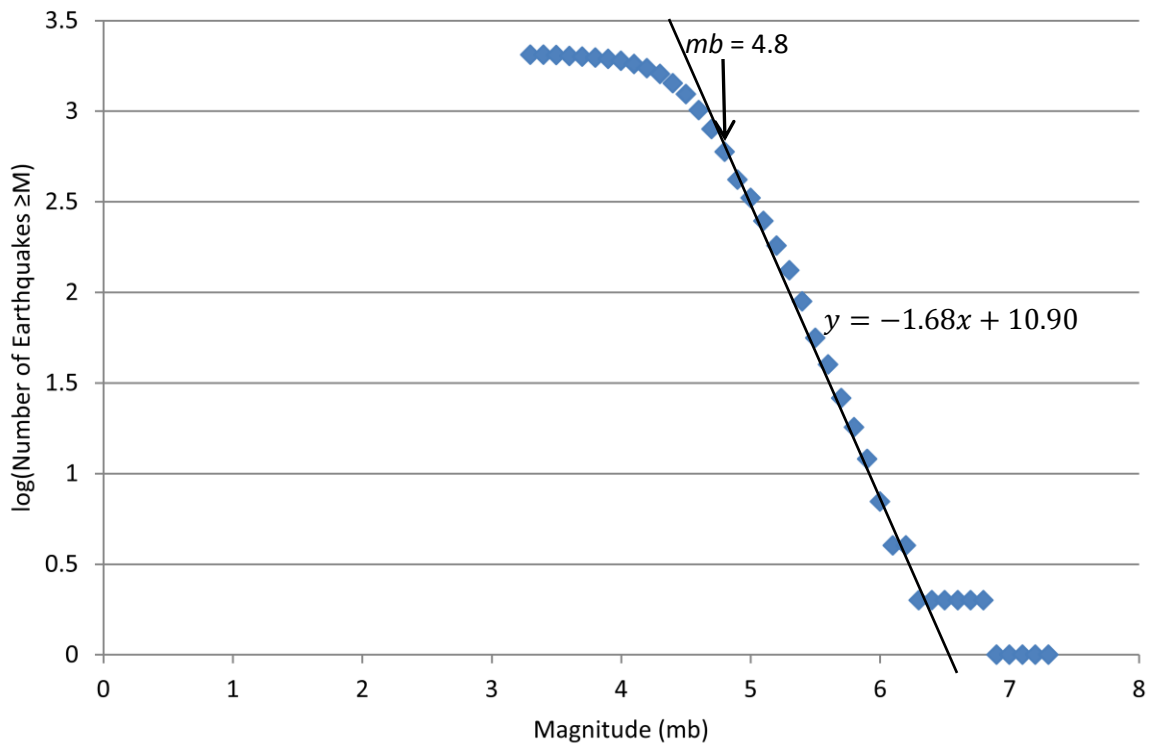


Figure A6: Gutenberg-Richter Plot for North Mid-Atlantic ridge (between 58°N and 19°N). The $mb = 4.8$ point on the plot shows where the distribution deviates away from a linear trend.

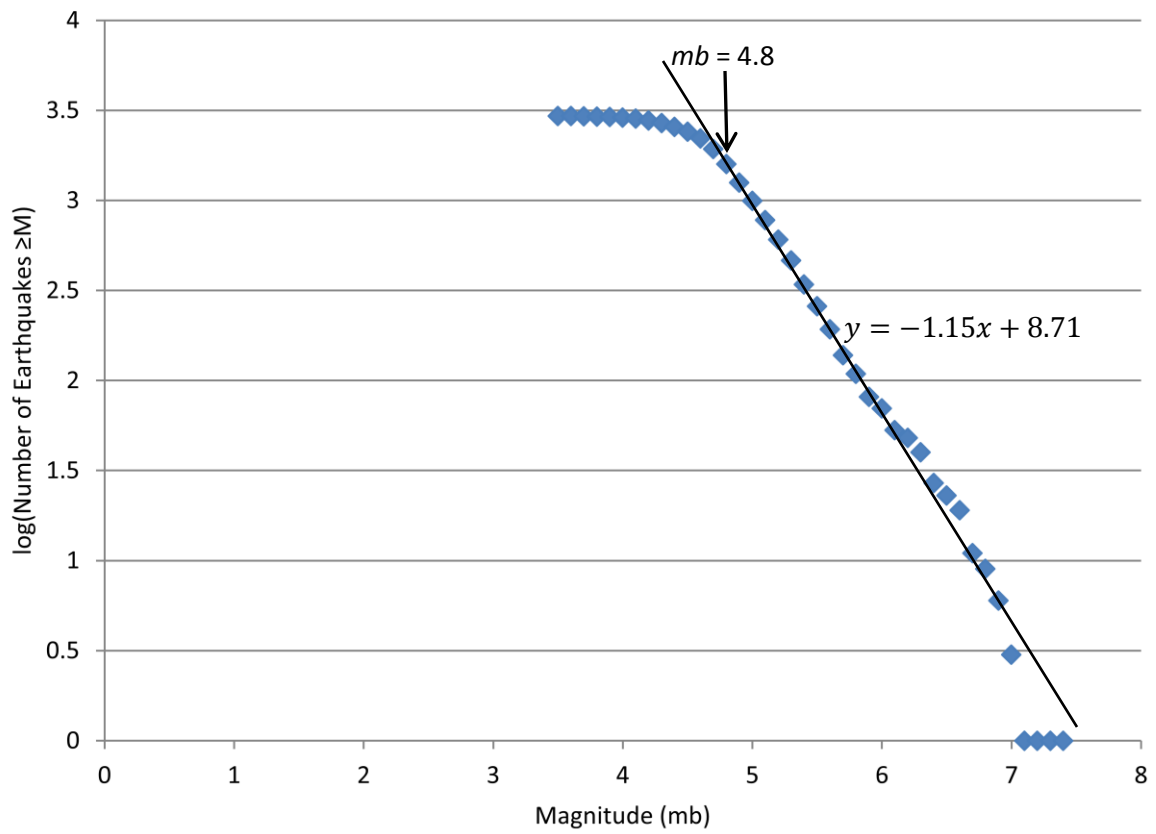


Figure A7: Gutenberg-Richter Plot for South Mid-Atlantic ridge (between 19°N and 38°S). The $mb = 4.8$ point on the plot shows where the distribution deviates away from a linear trend.

Appendix B: Supplemental tables that were referred to in section 5.

Table B1: The result from the test of Latchman (2011) observation on the MAR and ACM.

MAR Event serial number	Number of margin event within Latchman (2011) time window	Total number of margin events	Observed Rate	Mean Rate given a Poisson distribution	Difference between the observed and mean rates
1	10	315	15	8.07692308	6.92307692
2	2	320	3	8.20512821	-5.2051282
3	24	1085	36	27.8205128	8.17948718
4	39	1082	58.5	27.7435897	30.7564103
5	0	1081	0	27.7179487	-27.717949
6	19	1081	28.5	27.7179487	0.78205128
7	260	1040	390	26.6666667	363.333333
8	0	1017	0	26.0769231	-26.076923
9	16	1000	24	25.6410256	-1.6410256
10	17	880	25.5	22.5641026	2.93589744
11	25	159	37.5	4.07692308	33.4230769
12	0	59	0	1.51282051	-1.5128205
13	1	139	1.5	3.56410256	-2.0641026
14	5	1846	7.5	47.3333333	-39.833333
15	0	1846	0	47.3333333	-47.333333

16	15	2089	22.5	53.5641026	-31.064103
17	1	3509	1.5	89.974359	-88.474359
18	1	3509	1.5	89.974359	-88.474359
19	12	4845	18	124.230769	-106.23077
20	307	5682	460.5	145.692308	314.807692
21	440	5633	660	144.435897	515.564103
22	18	5633	27	144.435897	-117.4359
23	13	5605	19.5	143.717949	-124.21795
24	235	5605	352.5	143.717949	208.782051
25	365	5583	547.5	143.153846	404.346154
26	85	2415	127.5	61.9230769	65.5769231
27	78	1833	117	47	70
28	34	1833	51	47	4
29	0	1833	0	47	-47
30	2	1793	3	45.974359	-42.974359
31	12	1522	18	39.025641	-21.025641
32	0	1477	0	37.8717949	-37.871795
33	6	1477	9	37.8717949	-28.871795
34	18	1009	27	25.8717949	1.12820513
35	5	215	7.5	5.51282051	1.98717949
36	8	156	12	4	8
37	3	156	4.5	4	0.5
38	7	156	10.5	4	6.5
39	7	150	10.5	3.84615385	6.65384615

40	3	150	4.5	3.84615385	0.65384615
41	4	147	6	3.76923077	2.23076923
42	0	147	0	3.76923077	-3.7692308
43	2	134	3	3.43589744	-0.4358974
44	0	134	0	3.43589744	-3.4358974
45	3	121	4.5	3.1025641	1.3974359
46	2	119	3	3.05128205	-0.0512821
47	0	119	0	3.05128205	-3.0512821
48	1	119	1.5	3.05128205	-1.5512821
49	1	119	1.5	3.05128205	-1.5512821
50	1	119	1.5	3.05128205	-1.5512821
51	0	119	0	3.05128205	-3.0512821
52	2	117	3	3	0
53	1	117	1.5	3	-1.5
54	0	117	0	3	-3
55	7	117	10.5	3	7.5
56	7	117	10.5	3	7.5
57	0	116	0	2.97435897	-2.974359
58	1	116	1.5	2.97435897	-1.474359
59	2	115	3	2.94871795	0.05128205
60	1	115	1.5	2.94871795	-1.4487179
61	0	115	0	2.94871795	-2.9487179
62	0	115	0	2.94871795	-2.9487179
63	1	115	1.5	2.94871795	-1.4487179

64	0	115	0	2.94871795	-2.9487179
65	2	115	3	2.94871795	0.05128205
66	0	115	0	2.94871795	-2.9487179
67	0	115	0	2.94871795	-2.9487179
68	1	115	1.5	2.94871795	-1.4487179
69	0	114	0	2.92307692	-2.9230769
70	1	116	1.5	2.97435897	-1.474359
71	0	115	0	2.94871795	-2.9487179
72	1	115	1.5	2.94871795	-1.4487179
73	7	115	10.5	2.94871795	7.55128205
74	7	112	10.5	2.87179487	7.62820513
75	0	112	0	2.87179487	-2.8717949
76	0	20	0	0.51282051	-0.5128205
77	0	20	0	0.51282051	-0.5128205
78	0	20	0	0.51282051	-0.5128205
79	1	4	1.5	0.1025641	1.3974359
80	0	4	0	0.1025641	-0.1025641
81	1	4	1.5	0.1025641	1.3974359
82	0	4	0	0.1025641	-0.1025641
83	0	4	0	0.1025641	-0.1025641
84	0	4	0	0.1025641	-0.1025641
85	1	4	1.5	0.1025641	1.3974359
86	0	4	0	0.1025641	-0.1025641
87	0	3	0	0.07692308	-0.0769231

88	0	3	0	0.07692308	-0.0769231
----	---	---	---	------------	------------

Table B2: The result from the test of the Latchman (2011) observation on the MAR and Atlantic Basin.

MAR Event serial number	Number of margin event within Latchman (2011) time window	Total number of margin events	Observed Rate	Mean Rate given a Poisson distribution	Difference between the observed and mean rates
1	0	5	0	0.128205	-0.12821
2	0	5	0	0.128205	-0.12821
3	0	136	0	3.487179	-3.48718
4	1	136	1.5	3.487179	-1.98718
5	0	131	0	3.358974	-3.35897
6	4	132	6	3.384615	2.615385
7	0	135	0	3.461538	-3.46154
8	2	135	3	3.461538	-0.46154
9	0	135	0	3.461538	-3.46154
10	5	121	7.5	3.102564	4.397436
11	12	62	18	1.589744	16.41026
12	1	44	1.5	1.128205	0.371795
13	3	49	4.5	1.25641	3.24359
14	1	52	1.5	1.333333	0.166667
15	0	52	0	1.333333	-1.33333
16	0	52	0	1.333333	-1.33333
17	0	51	0	1.307692	-1.30769
18	0	51	0	1.307692	-1.30769
19	0	51	0	1.307692	-1.30769
20	0	42	0	1.076923	-1.07692

21	0	33	0	0.846154	-0.84615
22	0	33	0	0.846154	-0.84615
23	0	32	0	0.820513	-0.82051
24	0	32	0	0.820513	-0.82051
25	0	32	0	0.820513	-0.82051
26	0	25	0	0.641026	-0.64103
27	0	24	0	0.615385	-0.61538
28	0	24	0	0.615385	-0.61538
29	0	24	0	0.615385	-0.61538
30	0	24	0	0.615385	-0.61538
31	0	24	0	0.615385	-0.61538
32	1	23	1.5	0.589744	0.910256
33	0	23	0	0.589744	-0.58974
34	0	19	0	0.487179	-0.48718
35	0	24	0	0.615385	-0.61538
36	0	26	0	0.666667	-0.66667
37	0	26	0	0.666667	-0.66667
38	0	26	0	0.666667	-0.66667
39	0	27	0	0.692308	-0.69231
40	1	27	1.5	0.692308	0.807692
41	0	27	0	0.692308	-0.69231
42	0	27	0	0.692308	-0.69231
43	0	27	0	0.692308	-0.69231
44	0	27	0	0.692308	-0.69231
45	0	27	0	0.692308	-0.69231
46	2	27	3	0.692308	2.307692
47	0	27	0	0.692308	-0.69231
48	0	27	0	0.692308	-0.69231
49	0	27	0	0.692308	-0.69231
50	0	27	0	0.692308	-0.69231

51	0	27	0	0.692308	-0.69231
52	0	27	0	0.692308	-0.69231
53	0	27	0	0.692308	-0.69231
54	0	27	0	0.692308	-0.69231
55	0	27	0	0.692308	-0.69231
56	1	27	1.5	0.692308	0.807692
57	0	27	0	0.692308	-0.69231
58	0	27	0	0.692308	-0.69231
59	0	28	0	0.717949	-0.71795
60	0	28	0	0.717949	-0.71795
61	2	28	3	0.717949	2.282051
62	0	28	0	0.717949	-0.71795
63	0	28	0	0.717949	-0.71795
64	0	28	0	0.717949	-0.71795
65	0	27	0	0.692308	-0.69231
66	0	27	0	0.692308	-0.69231
67	0	27	0	0.692308	-0.69231
68	0	27	0	0.692308	-0.69231
69	0	27	0	0.692308	-0.69231
70	0	27	0	0.692308	-0.69231
71	1	27	1.5	0.692308	0.807692
72	0	26	0	0.666667	-0.66667
73	0	26	0	0.666667	-0.66667
74	0	20	0	0.512821	-0.51282
75	0	20	0	0.512821	-0.51282
76	0	26	0	0.666667	-0.66667
77	0	23	0	0.589744	-0.58974
78	0	14	0	0.358974	-0.35897
79	0	21	0	0.538462	-0.53846
80	0	21	0	0.538462	-0.53846

81	0	21	0	0.538462	-0.53846
82	0	21	0	0.538462	-0.53846
83	0	21	0	0.538462	-0.53846
84	0	21	0	0.538462	-0.53846
85	0	21	0	0.538462	-0.53846
86	0	21	0	0.538462	-0.53846
87	0	21	0	0.538462	-0.53846
88	0	21	0	0.538462	-0.53846